



A plastic SQSTM1/p62-dependent autophagic reserve maintains proteostasis and determines proteasome inhibitor susceptibility in multiple myeloma cells

Enrico Milan, Tommaso Perini, Massimo Resnati, Ugo Orfanelli, Laura Oliva, Andrea Raimondi, Paolo Cascio, Angela Bachi, Magda Marcatti, Fabio Ciceri & Simone Cenci

To cite this article: Enrico Milan, Tommaso Perini, Massimo Resnati, Ugo Orfanelli, Laura Oliva, Andrea Raimondi, Paolo Cascio, Angela Bachi, Magda Marcatti, Fabio Ciceri & Simone Cenci (2015) A plastic SQSTM1/p62-dependent autophagic reserve maintains proteostasis and determines proteasome inhibitor susceptibility in multiple myeloma cells, *Autophagy*, 11:7, 1161-1178, DOI: [10.1080/15548627.2015.1052928](https://doi.org/10.1080/15548627.2015.1052928)

To link to this article: <http://dx.doi.org/10.1080/15548627.2015.1052928>



© 2015 The Author(s). Published with license by Taylor & Francis Group, LLC
Enrico Milan, Tommaso Perini, Massimo Resnati, Ugo Orfanelli, Laura Oliva, Andrea Raimondi, Paolo Cascio, Angela Bachi, Magda Marcatti, Fabio Ciceri, and Simone Cenci



Accepted author version posted online: 04 June 2015



View supplementary material [↗](#)



Submit your article to this journal [↗](#)



Article views: 811



View related articles [↗](#)



View Crossmark data [↗](#)



Citing articles: 1 View citing articles [↗](#)

A plastic SQSTM1/p62-dependent autophagic reserve maintains proteostasis and determines proteasome inhibitor susceptibility in multiple myeloma cells

Enrico Milan,^{1,2,#} Tommaso Perini,^{1,2,3,#} Massimo Resnati,¹ Ugo Orfanelli,¹ Laura Oliva,¹ Andrea Raimondi,⁴ Paolo Cascio,⁵ Angela Bachi,⁶ Magda Marcatti,³ Fabio Ciceri,³ and Simone Cenci^{1,2,*}

¹San Raffaele Scientific Institute; Division of Genetics and Cell Biology; Milan, Italy; ²Università Vita-Salute San Raffaele; Milan, Italy; ³San Raffaele Scientific Institute; Department of Oncohematology; Hematology and Bone Marrow Transplantation Unit; Milan, Italy; ⁴San Raffaele Scientific Institute; Imaging Research Center; Milan, Italy; ⁵Department of Veterinary Sciences; University of Torino; Torino, Italy; ⁶IFOM; FIRC Institute of Molecular Oncology; Milan, Italy

[#]These authors contributed equally to this work.

Keywords: aggregate, autophagy, bortezomib, endoplasmic reticulum, multiple myeloma, p62, plasma cells, proteasome, proteasome inhibitors, proteostasis, SQSTM1, ubiquitin

Abbreviations: Ab, antibody; amc, 7-amino-4-methylcoumarin; APC, allophycocyanin; Baf A1, bafilomycin A₁; Btz, bortezomib; BM, bone marrow; ER, endoplasmic reticulum; ERGIC, ER-Golgi intermediate compartment; GO, gene ontology; HCQ, hydroxychloroquine; Ig, immunoglobulin; IP, immunoprecipitation; LC-MS/MS, liquid chromatography–tandem mass spectrometry; MM, multiple myeloma; pAb, polyclonal antibody; PBS, phosphate-buffered saline; PC, plasma cell; PI, proteasome inhibitor; Rapa, rapamycin; SILAC, stable isotope labeling in cell culture; Ub, ubiquitin; UPR, unfolded protein response; UPS, ubiquitin-proteasome system.

Multiple myeloma (MM) is the paradigmatic proteasome inhibitor (PI) responsive cancer, but many patients fail to respond. An attractive target to enhance sensitivity is (macro)autophagy, recently found essential to bone marrow plasma cells, the normal counterpart of MM. Here, integrating proteomics with hypothesis-driven strategies, we identified the autophagic cargo receptor and adapter protein, SQSTM1/p62 as an essential component of an autophagic reserve that not only synergizes with the proteasome to maintain proteostasis, but also mediates a plastic adaptive response to PIs, and faithfully reports on inherent PI sensitivity. Lentiviral engineering revealed that SQSTM1 is essential for MM cell survival and affords specific PI protection. Under basal conditions, SQSTM1-dependent autophagy alleviates the degradative burden on the proteasome by constitutively disposing of substantial amounts of ubiquitinated proteins. Indeed, its inhibition or stimulation greatly sensitized to, or protected from, PI-induced protein aggregation and cell death. Moreover, under proteasome stress, myeloma cells selectively enhanced SQSTM1 de novo expression and reset its vast endogenous interactome, diverting SQSTM1 from signaling partners to maximize its association with ubiquitinated proteins. Saturation of such autophagic reserve, as indicated by intracellular accumulation of undigested SQSTM1-positive aggregates, specifically discriminated patient-derived myelomas inherently susceptible to PIs from primarily resistant ones. These aggregates correlated with accumulation of the endoplasmic reticulum, which comparative proteomics identified as the main cell compartment targeted by autophagy in MM. Altogether, the data integrate autophagy into our previously established proteasome load-versus-capacity model, and reveal SQSTM1 aggregation as a faithful marker of defective proteostasis, defining a novel prognostic and therapeutic framework for MM.

© Enrico Milan, Tommaso Perini, Massimo Resnati, Ugo Orfanelli, Laura Oliva, Andrea Raimondi, Paolo Cascio, Angela Bachi, Magda Marcatti, Fabio Ciceri, and Simone Cenci

*Correspondence to: Simone Cenci; Email: cenci.simone@hsr.it

Submitted: 09/30/2014; Revised: 05/05/2015; Accepted: 05/14/2015

<http://dx.doi.org/10.1080/15548627.2015.1052928>

This is an Open Access article distributed under the terms of the Creative Commons Attribution-Non-Commercial License (<http://creativecommons.org/licenses/by-nc/3.0/>), which permits unrestricted non-commercial use, distribution, and reproduction in any medium, provided the original work is properly cited. The moral rights of the named author(s) have been asserted.

Introduction

Multiple myeloma (MM) is the paradigmatic cancer susceptible to proteasome inhibitors (PIs), prototypical negative proteostasis regulators.¹ Accumulation of ubiquitin-protein conjugates is a crucial mechanism in PI toxicity.^{2,3} Normal plasma cells (PCs) acquire extreme vulnerability to PIs during their differentiation, due to a dramatic reduction of proteasome capacity, which does not meet the increased load of misfolded proteins requiring proteasomal degradation, thereby triggering stress and lowering the apoptotic threshold.⁴ This load-versus-capacity model contributes to explain PI sensitivity in malignant PCs, as myelomas with high proteasome capacity and low proteasome workload show relative primary resistance.⁵ Indicative of cause-effect relationships, both increasing proteasome expression⁵ and attenuating protein synthesis⁶ specifically reduced vulnerability of myeloma cells to the first-in-class PI bortezomib.

Despite the undisputed benefits of PIs, a proportion of PI-naïve patients fail to respond,⁷⁻⁹ establishing a strong need to develop biomarkers to identify patients more likely to benefit from PI-based therapy. Notably, such biomarkers may offer targets for novel therapeutic approaches to achieve higher efficacy, prevent side effects, and overcome resistance.^{2,10-12}

Macroautophagy, conventionally referred to as autophagy, is a conserved self-digestive lysosomal recycling pathway that sustains cell metabolism under conditions of nutrient deprivation.¹³⁻¹⁵ Autophagy also mediates selective degradation of intracellular supramolecular structures, including microbes (xenophagy), protein aggregates (aggrephagy), and organelles, thereby affording innate defense, maintaining protein homeostasis (proteostasis), and exerting critical quality control functions.^{16,17} In adaptive immunity, selective autophagy mediates key tissue-specific functions, including antigen presentation and T cell development.^{18,19} Recently, we discovered that autophagy is essential to ensure sustainable immunoglobulin (Ig) production in PCs, through the selective restriction of the endoplasmic reticulum (ER).²⁰ Other groups have independently confirmed the essential role of autophagy in sustaining antibody responses.²¹ Moreover, we found that autophagy is absolutely required to maintain the resident pool of bone marrow (BM) long-lived PCs, the normal counterpart of MM.²⁰

Autophagy is thought to play a 2-sided, context-dependent role in cancer biology, oncosuppressive in normal cells, and protumoral in established cancers, which may exploit autophagy to resist stress.²² In cellular and animal models of proteotoxicity, autophagy compensates for proteasome insufficiency by clearing protein aggregates.^{15,23,24} Myeloma cells are thus thought to be particularly dependent on autophagy owing to their distinctive overloaded ubiquitin (Ub)-proteasome system (UPS).¹⁰⁻¹² Hence, defining the constitutive levels, exact homeostatic functions and molecular mechanisms of autophagy in MM cells is needed to design specific strategies to disarm this cancer.

Selective autophagic degradation is achieved through proteins that act as specific cargo receptors, which crosslink the substrate with the autophagic machinery. The prototypical receptor, SQSTM1/p62, is a multifunctional signaling adapter protein

that has been implicated in a number of selective autophagic processes.¹⁷

In the present work, we investigated the role of SQSTM1 in the maintenance of protein homeostasis in MM cells. By combining unbiased proteomics and hypothesis-driven technologies, we identified a SQSTM1-dependent autophagic reserve that not only cooperates with the UPS for the clearance of Ub-protein conjugates, but is also capable of adapting to proteasome stress, through enhanced SQSTM1 expression and a profound reshaping of its interactome, revealing a tighter collaboration between the UPS and autophagy than previously thought. As a result, SQSTM1 is critical for MM cell survival, and its inhibition sensitizes to PIs. Moreover, the presence of SQSTM1-containing protein aggregates emerges as a novel potential biomarker of PI susceptibility of therapeutic and prognostic value.

Results

Intense autophagy constitutively degrades ubiquitinated proteins to prevent accumulation of SQSTM1-positive protein aggregates in myeloma cells

To quantify overall autophagic activity in MM cells, we assessed the rate of lysosomal digestion of lipidated, autophagosome-bound MAP1LC3A/LC3A (LC3A-II) in a panel of 6 MM lines. All 6 cell lines showed intense autophagic fluxes (Fig. 1A). In particular, their autophagic activity was 5- to 50-times higher than in the B lymphomas MEC1 (Fig. 1A) and RAJI (not shown). Stable lentiviral silencing of the essential autophagic molecule ATG7 confirmed the critical role of autophagy in maintaining MM cell survival (Fig. S1).^{25,26}

To address the function of such intense constitutive autophagy, we asked if it mediates the clearance of Ub-conjugated proteins in MM cells. Distal pharmacological inhibition of autophagy induced remarkable accumulation of heterogeneous ubiquitinated proteins and of the prototypical autophagic receptor, SQSTM1 (Fig. 1B). Immunofluorescence experiments revealed Ub-protein aggregates that colocalized with SQSTM1 (Fig. 1C). Moreover, autophagy blockade led to a remarkable increase in the number and size of SQSTM1⁺ cytoplasmic aggregates (Fig. 1D), and induced substantial accumulation of SQSTM1 in detergent-insoluble cellular fractions (Fig. 1E). The data demonstrate abundant and constitutive autophagic clearance of ubiquitinated proteins in MM cells, and suggest SQSTM1 as the receptor involved in such clearance.

Collaboration of the proteasome and autophagy to maintain protein homeostasis and viability of MM cells

The finding that autophagy constitutively contributes substantial clearance of ubiquitinated proteins suggests that it may play a crucial role in alleviating proteasome stress in MM cells, if substrates were shared with the UPS. To test this hypothesis, we attempted to increase or reduce PI toxicity, respectively, by weakening or empowering autophagy. Treatment with nontoxic doses of bortezomib and the distal autophagy inhibitor leupeptin yielded dramatic accumulation of Ub-protein conjugates and

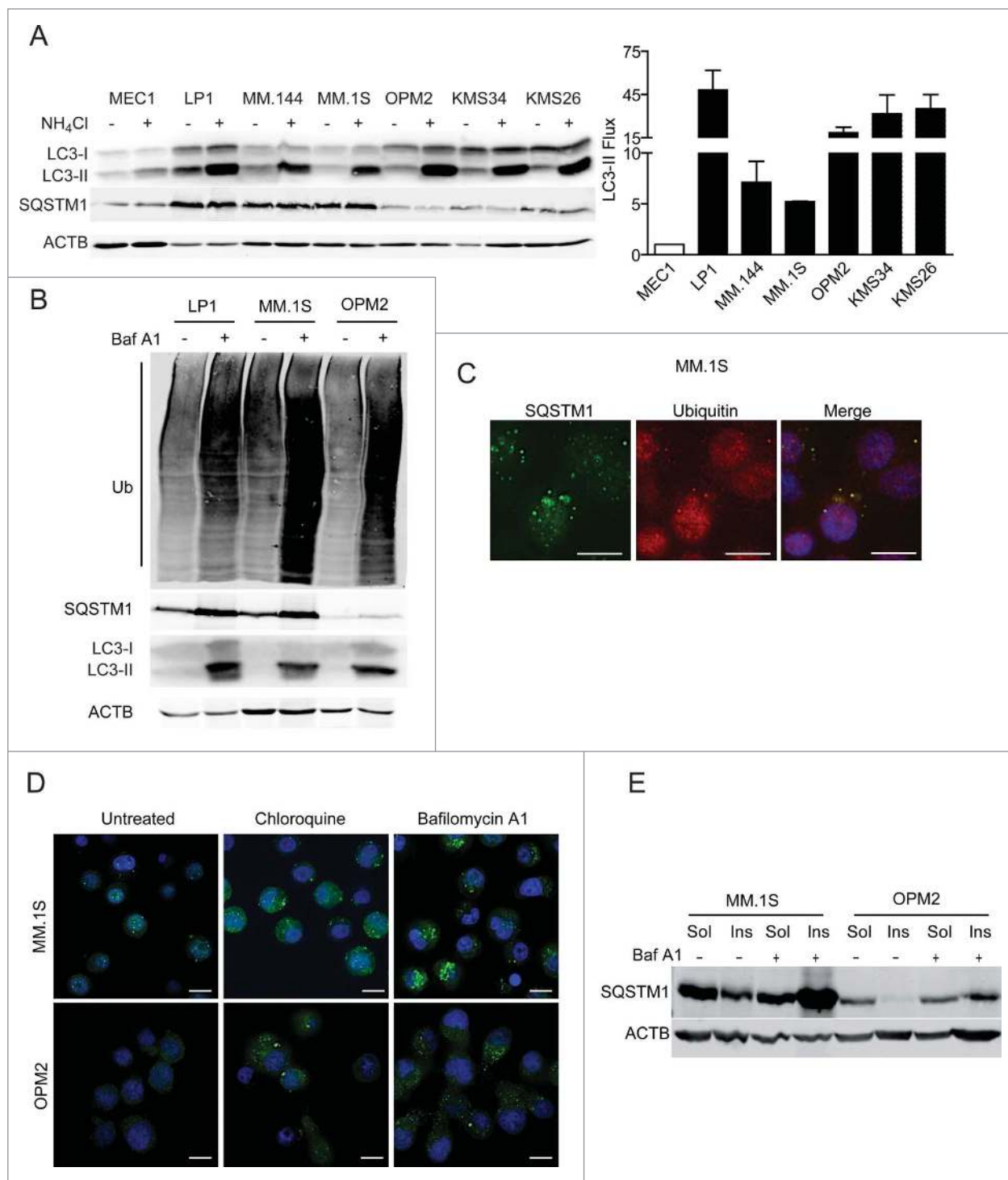


Figure 1. Autophagy inhibition leads to accumulation of SQSTM1⁺ undigested protein aggregates in MM cells. **(A)** Immunoblot analysis of endogenous unconjugated LC3-I to lipid-conjugated LC3-II and SQSTM1 in multiple myeloma (MM) cell lines. The MEC1 lymphoma and the indicated MM cell lines were treated for 2 h with 50 mM NH₄Cl or left untreated, lysed in 1% SDS and analyzed by western blot with anti-LC3 Ab (left). ACTB/actin serves as a loading control throughout. Right, autophagic flux quantified as the difference of LC3-II band intensity with and without NH₄Cl, normalized on MEC1 values (average \pm s.e.m., n = 5). **(B)** Immunoblot analysis of ubiquitinated proteins, SQSTM1 and LC3 in MM cells treated with 100 nM bafilomycin A₁ (Baf A1) for 24 h (representative image, n = 3). **(C)** Immunofluorescence analysis of SQSTM1 (green) and ubiquitin (red) in MM.1S cells. Nuclei are stained blue with DAPI. Scale bars: 10 μ m. **(D)** Immunofluorescence analysis of SQSTM1 and ubiquitin in MM.1S and OPM2 cells treated with chloroquine (50 μ M) or bafilomycin A₁ (100 nM) for 24 h. Nuclei are stained blue with DAPI. Scale bars; 10 μ m. **(E)** Representative immunoblot analysis of SQSTM1 in MM cells treated with 100 nM Baf A1 for 24 h and lysed in 1% NP-40. Insoluble material was treated with 1% SDS and the DNA was sonicated. NP-40 soluble and insoluble fractions were quantified and equal protein amounts resolved by SDS-PAGE.

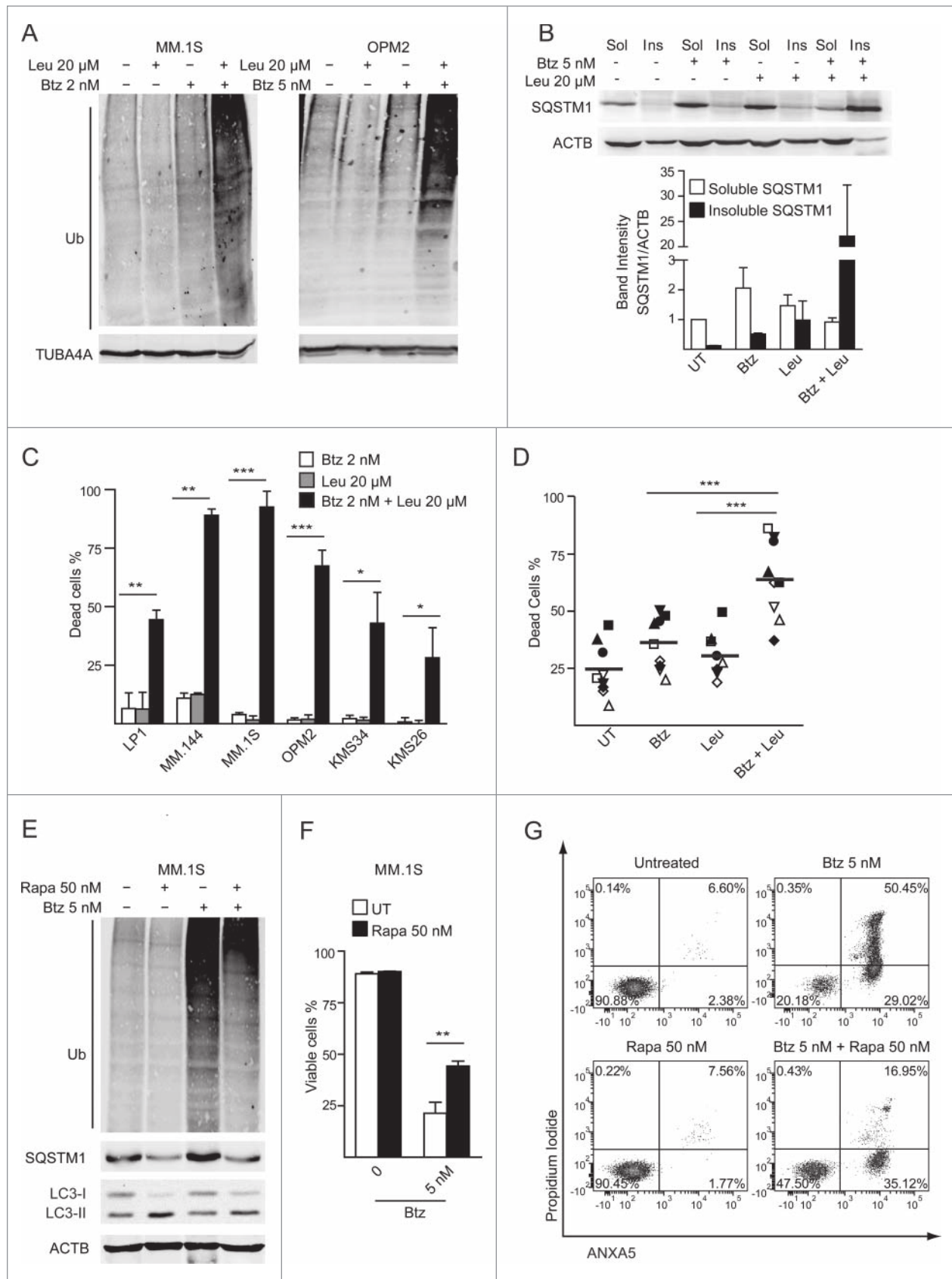


Figure 2. For figure legend, see page 1165.

insoluble SQSTM1 (Fig. 2A–B), which preceded massive synergistic cell death in MM lines (Fig. 2C) and in primary, patient-derived MM cells (Fig. 2D). Conversely, stimulation of autophagy substantially prevented PI-induced accumulation of Ub-proteins (Fig. 2E) and the subsequent death of MM cells (Fig. 2F–G). The data establish that in myeloma cells autophagy cooperates with the proteasome, sharing Ub-protein substrates, and limits PI sensitivity. However, in our hands, autophagic inhibition by lentiviral *ATG7* silencing or by hydroxychloroquine (HCQ) caused minor increases of bortezomib-induced toxicity in MM cell lines (Figs. S1F and S2). The data also suggest that, by integrating stress of both the UPS and autophagy, accumulation of insoluble SQSTM1 (Fig. 2B and E) may predict proteotoxicity.

SQSTM1 is essential to myeloma cells and yields specific protection against proteasome inhibitors

In view of the tight cooperation of the UPS and autophagy documented in MM cells, we next challenged the relevance of SQSTM1 in myeloma cell viability and PI sensitivity. To this aim, we achieved stable *SQSTM1* silencing by lentiviral shRNA expression. Reduction of SQSTM1 protein abundance in MM cell lines (Fig. 3A and Fig. S3A) induced significant decrease of intracellular ATP (Fig. 3B) and remarkable toxicity, with massive death of *SQSTM1*-silenced MM lines in less than 2 wk, as assessed by apoptosis and colony-forming assays (Fig. 3C, D and Fig. S3B). Conversely, a comparable reduction of SQSTM1 expression in 2 B lymphomas elected as controls (Fig. 3A) induced significantly less or negligible death (Fig. 3C), suggesting that SQSTM1 requirement is specific to PCs. We then exploited the timeframe preceding overt toxicity to test if SQSTM1 confers specific protection against PIs. Prior to the onset of cell death, *SQSTM1*-silenced MM cells revealed significantly increased susceptibility to bortezomib-induced accumulation of ubiquitinated proteins and toxicity (Fig. 3E, F and Fig. S3C). The protective activity of SQSTM1 was specific, as its reduction failed to affect the toxicity of the distinct anti-myeloma agent doxorubicin (Fig. 3F). Thus, MM cells require SQSTM1 for survival and specific inherent resistance to PIs.

Proteasome stress co-opts SQSTM1 onto protein aggregates and induces de novo SQSTM1 expression

The increased sensitivity of *SQSTM1*-silenced MM cells to PIs urged us to address the mechanisms whereby SQSTM1 mediates

PI resistance in MM cells. Along with its role as an autophagic receptor, SQSTM1 is a multi-tasking adapter protein regulating multiple signaling pathways. We thus examined its expression, distribution, and activity under proteasome stress. Short (1 h) treatment with a high dose (1 μ M) of the first-in-class PI bortezomib induced the appearance of large (\sim 100 nm to $>$ 1 μ m) SQSTM1⁺ aggregates in MM cells (Fig. 4A), with a Ub⁺ core surrounded by SQSTM1 (Fig. 4B). Immunoprecipitation (IP) experiments demonstrated the specific interaction of SQSTM1 and ubiquitinated proteins. Such interaction was magnified by PIs, while the prototypic interaction with KEAP1, which promotes NFE2L2/NRF2-dependent anti-oxidant responses, was greatly reduced (Fig. 4C). We then adopted stable isotope labeling in cell culture (SILAC) proteomics to precisely quantify the changes of the SQSTM1 interactome upon proteasome inhibition (experimental design illustrated in Fig. S4A, B). Under basal conditions, SQSTM1 bound a number of known interactors, e.g., KEAP1, PRKCI, and Ub (Table 1). Noticeably, proteasome inhibition induced a dramatic change of the SQSTM1 interactome, with Ub increasing by \sim 10 times, at the expense of other interactors (Fig. 4D and Table 1). Moreover, SQSTM1 expression analyses revealed that bortezomib also selectively increased de novo expression of SQSTM1, but not of the autophagic receptors NBR1 and OPTN/optineurin, as demonstrated by increased transcript and protein levels (Fig. 4E, F and Fig. S4C), an effect independent of autophagy (attested to by no consistent change in LC3 conversion in Fig. 4F) and completely prevented by inhibition of protein translation (Fig. 4G). Together, the data reveal a previously unrecognized 2-fold adaptive response deployed by MM cells under proteasome stress, consisting of rapid co-opting of SQSTM1 onto Ub-protein aggregates, at the expense of its signaling activities, and enhanced SQSTM1 expression.

SQSTM1⁺ protein aggregates specifically predict proteasome inhibitor susceptibility in MM lines and patient-derived myelomas

Having identified a key protective role for SQSTM1 in mediating the autophagic degradation of proteasome-undigested Ub-proteins in MM cells (Fig. 4), and in view of the strong correlation between SQSTM1 aggregation and subsequent toxicity observed in vitro (Fig. 2), we then explored the prognostic significance of SQSTM1 as a biomarker of primary PI susceptibility. This idea stemmed from 2 observations: first, that PI-sensitive

Figure 2 (See previous page). The proteasome and autophagy synergize to maintain protein homeostasis and viability of MM cells. (A–D) Inhibition of autophagy sensitizes MM cells to PI-induced accumulation of Ub-proteins and cell death. (A) Immunoblot analysis of ubiquitinated proteins in MM lines treated with the indicated doses of bortezomib (Btz) and leupeptin (Leu), alone or combined, for 24 h (representative blots of 3 independent experiments). (B) Immunoblot analysis of SQSTM1 in OPM2 cells left untreated or treated for 24 h with the indicated doses of Btz and Leu (20 μ M), alone or combined. Equal amounts of NP-40 soluble and insoluble fractions were loaded and resolved by SDS-PAGE. Top, representative blots; bottom, quantification of 3 independent experiments (average \pm s.e.m.). (C) MM lines were treated with the indicated doses of Btz and Leu, alone or combined, for 48 h, and cell viability assessed by flow cytometry upon propidium iodide and ANXA5 staining (average quantification of ANXA5 positive cells \pm s.e.m., n = 4). (D) MM cells were immunomagnetically sorted from BM aspirates obtained from newly diagnosed patients treated for 24 h with 2 or 5 nM Btz and 10 μ M Leu, alone or combined, and cell viability assessed by flow cytometry after staining with propidium iodide and ANXA5 (average quantification of ANXA5-positive cells \pm s.e.m.; n = 9 patients). (E–G) Stimulation of autophagy protects MM cells from PI-induced build-up of ubiquitinated proteins and cell death. (E) Immunoblot analysis of SQSTM1, LC3 and ubiquitinated proteins in MM.1S cells treated for 24 h with the indicated dose of rapamycin (Rapa), in the presence or absence of bortezomib (Btz) for the last 8 h (n = 3). (F) The viability of cells treated as in (E) for 24 h was assessed by flow cytometry upon propidium iodide and ANXA5 staining (average quantification of double negative cells \pm s.e.m., n = 4). (G) Representative density plot of propidium iodide and ANXA5 staining in Rapa and/or Btz-treated MM.1S cells. **P* < 0.05; ***P* < 0.01; ****P* < 0.001; unpaired Student *t* test.

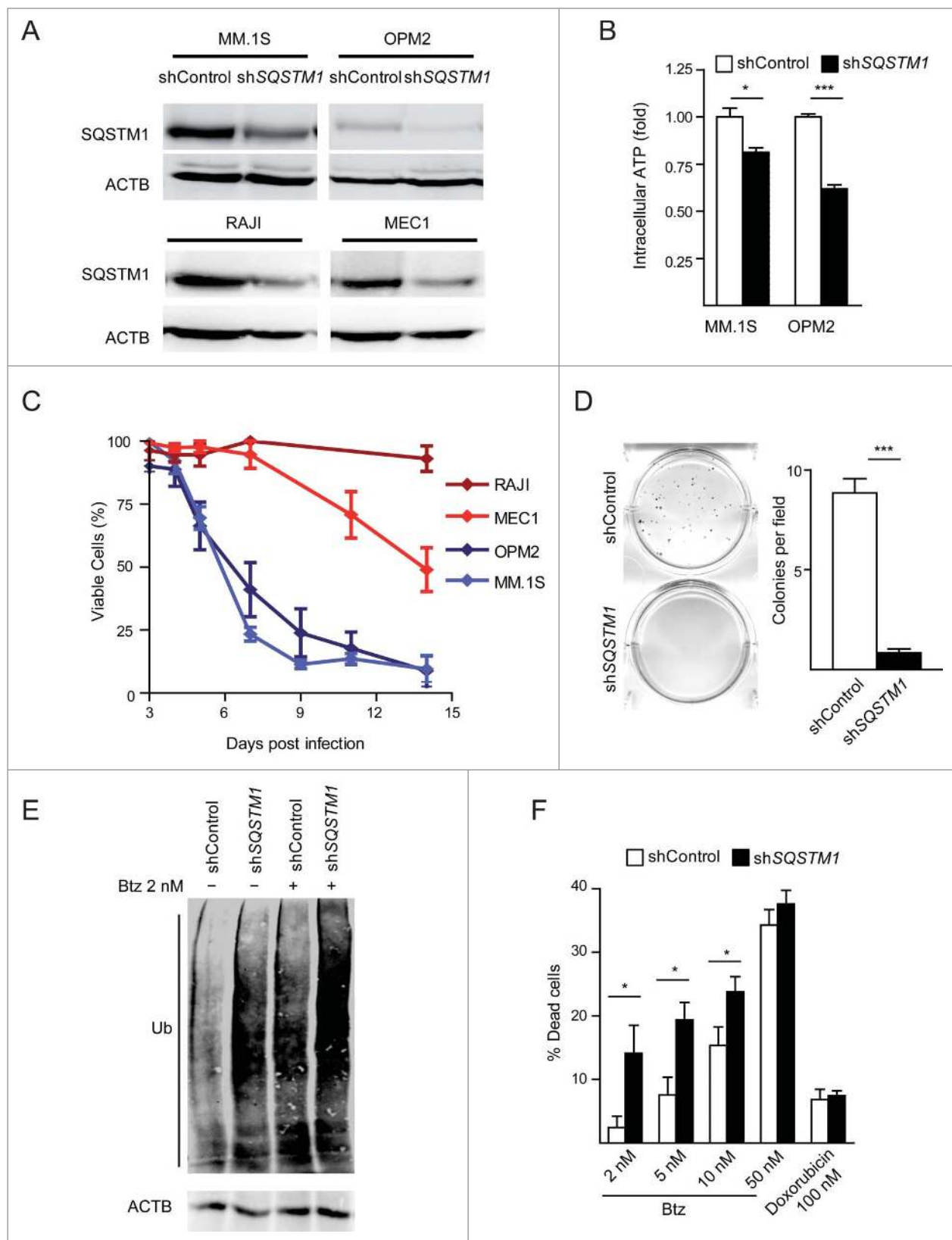


Figure 3. For figure legend, see page 1167.

MM.1S cells displayed SQSTM1⁺ aggregates in basal conditions, whereas relatively resistant OPM2 cells did not (Fig. 1); second, that SQSTM1 aggregation preceded cell death upon treatment with toxic doses of proteasome and autophagy inhibitors, alone or in combination (Fig. 2). Hence, we hypothesized that SQSTM1 aggregation could serve as a reliable marker of insufficient autophagic reserve and proteotoxicity.

To test this hypothesis, we extended the immunofluorescence and biochemical analyses of SQSTM1 accumulation to a panel of 11 MM lines, hallmarked by differential intrinsic sensitivity to bortezomib, as determined in standard 24-h apoptotic response curves (Fig. S5A). Immunoblotting experiments showed remarkable accumulation of SQSTM1 in the lines characterized by lower EC₅₀ values (Fig. 5A, left panel and Fig. S5B). Moreover, we found SQSTM1 in detergent-insoluble fractions and in immunofluorescent aggregates exclusively in the most PI-sensitive lines (Fig. 5A, right, 5B, and Fig. S5C). Accumulation of SQSTM1⁺ aggregates specifically reported on defective proteostasis, as the average cell count of SQSTM1⁺ puncta in each line correlated significantly with the EC₅₀ of bortezomib (Fig. 5C), but not with that calculated with the distinct anti-myeloma agent, dexamethasone (Fig. 5D).

We then challenged the significance of SQSTM1⁺ puncta in primary MM cells purified from newly diagnosed MM patients. Notably, also in patient-derived cells, we could neatly discriminate between myelomas that do or do not display SQSTM1⁺ puncta (Fig. 5E). The presence of SQSTM1⁺ structures identified the myelomas with the highest susceptibility to bortezomib in vitro (i.e., EC₅₀ ≤ 5 nM) (Fig. 5F). Moreover, the average cellular count of SQSTM1⁺ puncta within each tumor population significantly correlated with the EC₅₀ of bortezomib determined in vitro (Fig. 5G). The coincidence of accumulation of SQSTM1⁺ aggregates with exquisite inherent PI sensitivity also in primary samples confirms saturation of a putative protective autophagic reserve. The data provide proof-of-principle evidence and pre-clinical validation of SQSTM1 aggregation as a single-cell indicator of intrinsic susceptibility to PIs.

A proteostatic autophagic reserve is saturated in PI-sensitive myelomas

The observation of SQSTM1 aggregation selectively in most PI-sensitive myelomas (Fig. 5) suggested the existence of a functional autophagic reserve saturated in basal conditions in those tumors. Indeed, when we challenged a panel of MM lines with

low dose (5 nM) bortezomib, relatively PI-resistant lines did not accumulate ubiquitinated proteins, while PI-sensitive cells did, despite the fact that comparable proteasome inhibition had been achieved (Fig. 6A, B). To test if this differential proteostatic reserve is accounted for by autophagy, we utilized pharmacological and genetic inhibition. In keeping with our hypothesis, immunofluorescent detection of SQSTM1⁺ puncta revealed defective autophagic clearance of bortezomib-induced aggregates in PI-sensitive MM lines (Fig. 6C, D). Immunoblotting experiments confirmed that bortezomib was sufficient to induce the accumulation of insoluble SQSTM1 in PI-sensitive MM lines, whereas the distal autophagy inhibitor bafilomycin A₁ was required to induce accumulation of insoluble SQSTM1 in PI-resistant cells (Fig. 6E). Indeed, in these cells, inhibition of autophagy, as achieved by cotreatment with leupeptin or by previous lentiviral *ATG7* RNAi, maximized the limited accumulation of ubiquitinated proteins induced by subtoxic proteasome stress (Fig. 6F). Together, these experiments formally demonstrate the existence, in MM cells, of an autophagic reserve required to cope with PI-induced proteotoxicity and maintain proteostasis, and that such reserve is saturated in PI-sensitive myelomas.

The ER is a major autophagic substrate that accumulates in PI-sensitive myelomas

The observation that SQSTM1-containing aggregates hallmark certain myelomas, but not all (Fig. 5), raises the question as to whether additional targets burden autophagy. We recently discovered that the ER is the main cell compartment degraded by autophagy in normal PCs.²⁰ To test if reticulophagy is a major autophagic task also in malignant PCs, we adopted an unbiased proteomic approach to define the cell compartments that are constitutive targets of autophagy in MM cells. We first studied OPM2 cells, in which SQSTM1 degradation and autophagy are most proficient, and then extended our observations to other cell lines. The proteome of OPM2 cells was labeled by SILAC and the changes of individual proteins upon pharmacological autophagy inhibition quantified by LC-MS/MS. We achieved distal autophagy blockade by treating MM cells for 24 h with the lysosomal inhibitor leupeptin at a dose that arrested the autophagic flux (Fig. S6A), causing no toxicity (loss of ATP or viability), no proteasome stress (accumulation of Ub-proteins), and no adaptive activation of the unfolded protein response (UPR) (Fig. S6B–E). In 2 different experiments with inverted isotope labeling, we identified 981 proteins with at least 2 peptides quantified

Figure 3 (See previous page). SQSTM1 is essential for MM cell survival and affords specific protection against proteasome inhibitors. (A) Immunoblot analysis of SQSTM1 in the indicated myeloma and lymphoma cell lines 4 d after infection with lentiviral vectors expressing anti-*SQSTM1* and control shRNAs (representative blots, n = 3). (B) Intracellular ATP in fresh lysates from OPM2 and MM.1S cells 4 d post *SQSTM1* silencing (average ± s.e.m., n = 4, normalized to cell number). (C) The indicated MM and B lymphoma cell lines were infected with lentiviruses co-expressing shRNA against *SQSTM1* or control shRNA, and GFP, and the percentage of live GFP⁺ cells expressing anti-*SQSTM1* shRNA was assessed at the indicated timepoints by flow cytometry upon propidium iodide and ANXA5 staining, and normalized by the frequency of live GFP⁺ cells expressing control shRNA. (D) Soft agar colony-forming assay on MM cells 4 d after lentiviral infection. After 21 d colonies were stained with thiazolyl blue tetrazolium bromide and counted by light microscopy (average number of colonies per field ± s.e.m.). (E) Immunoblot analysis of ubiquitinated proteins in OPM2 cells 4 d after lentiviral infection treated for 8 h with the indicated dose of bortezomib (n = 3). (F) Apoptotic sensitivity to 24 h treatment with the indicated doses of bortezomib and doxorubicin in GFP⁺ *SQSTM1*-silenced and control OPM2 cells was assessed by flow cytometry, as above, and expressed as the percentage of propidium iodide- and/or ANXA5-positive cells, normalized to untreated cells (n = 6). Similar results were obtained with MM.1S cells. *P < 0.05; ***P < 0.001; unpaired Student t test.

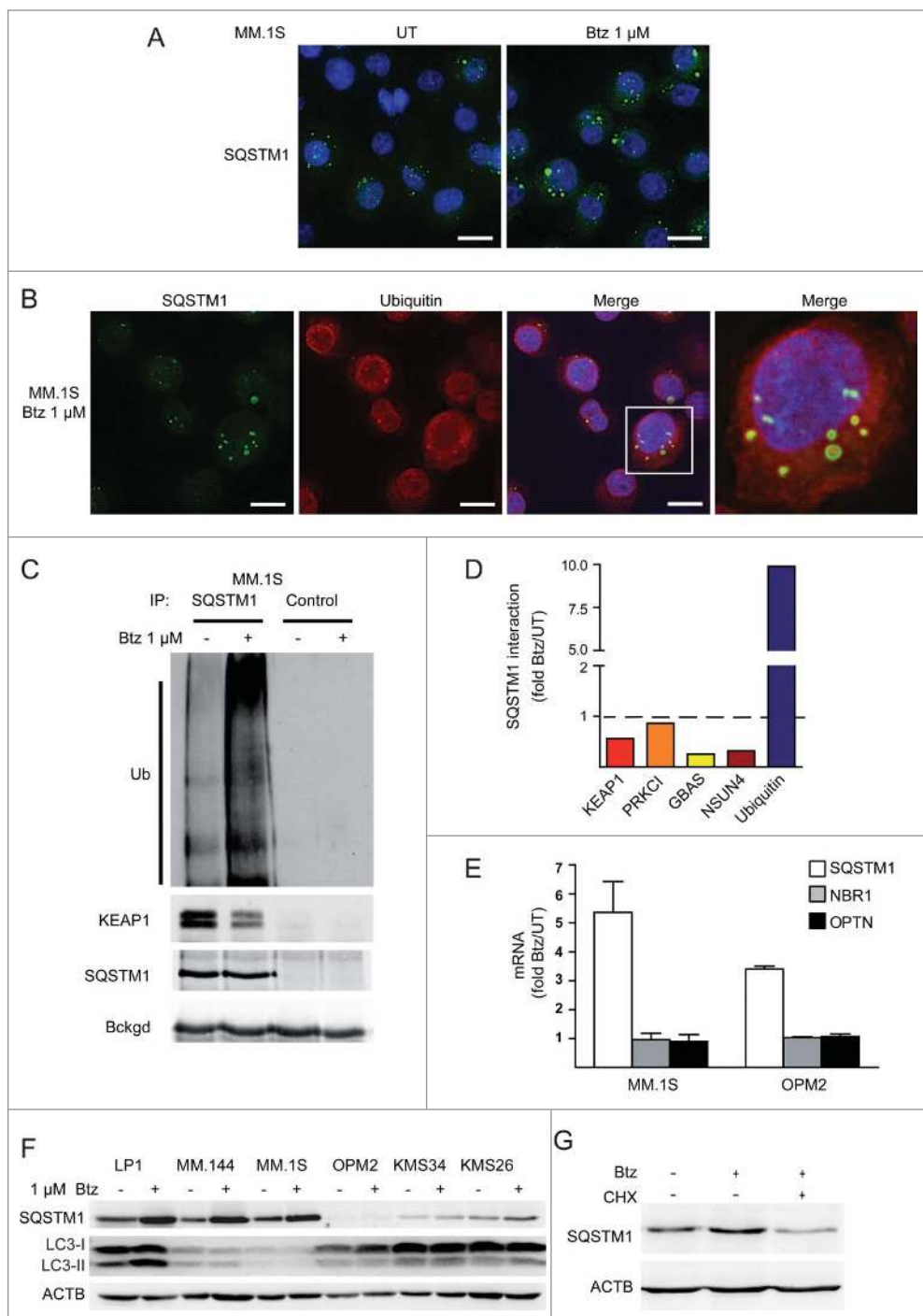


Figure 4. Acute proteasome stress co-opts SQSTM1 onto protein aggregates, and induces de novo SQSTM1 expression. (**A**, **B**) Immunofluorescence analysis of SQSTM1 and ubiquitin accumulation in MM lines upon treatment with bortezomib (Btz). Nuclei are stained blue with DAPI. Scale bars: 10 μ m. (**A**) SQSTM1 in MM.1S cells left untreated (left) or treated for 1 h with 1 μ M Btz (right) ($n = 5$ independent experiments). (**B**) SQSTM1 and ubiquitin in MM.1S cells treated with Btz (as in **A**). (**C**) Co-immunoprecipitation (IP) of poly-ubiquitinated proteins with SQSTM1. MM.1S cells were treated with Btz (as in **A**), prior to IP of SQSTM1, and the association of ubiquitinated proteins and KEAP1 with SQSTM1 assessed by immunoblot ($n \geq 3$). (**D**) Changes of selected proteins of the SQSTM1 interactome upon treatment with Btz (as in **A**) as determined by SILAC LC-MS/MS in MM.1S cells (more proteins listed in Table 1). (**E**) Quantitative RT-PCR analysis of transcripts encoding the indicated autophagy receptors in MM lines treated with 1 μ M Btz for 4 h. mRNA amounts were normalized by histone H3 and expressed relative to untreated controls (average induction \pm s.e.m.; $n = 3$). (**F**) Immunoblot analysis of SQSTM1 and LC3 in the indicated MM lines treated with 1 μ M Btz for 8 h (representative blot, $n = 3$). (**G**) Immunoblot analysis of SQSTM1 in MM.1S cells treated with 1 μ M Btz for 8 h in the presence or absence of 10 μ g/ml cycloheximide (CHX).

in both experiments (Dataset S1). We found 45 proteins consistently and significantly upregulated by leupeptin. These included established components of the secretory apparatus, such as LMAN1/ERGIC53, ERP44, and RAB7A (Table S1). Gene ontology (GO) analysis of upregulated proteins among the 981 quantified found significant specific enrichment of ER-resident proteins (GO:0005789; $p = 0.041$) and the Golgi apparatus (GO:0005794; $p = 0.039$), together with the expected lysosomal compartment (GO:0005764; $p = 0.024$). By extending the GO analysis to all quantified proteins, we found lysosomal inhibition

to induce a concerted, significant increase of ER membrane proteins ($n = 32$, average increase 4.3%), ERGIC ($n = 12$, average increase 7.6%) and Golgi ($n = 60$, average increase 6.6%). Conversely, no increase was found in ribosomal, nuclear and cytosolic proteins, whereas a slight, concerted increase was detected for mitochondrial proteins ($n = 167$, average increase 0.7%) (Fig. 7A). A significant increase of selected components of the secretory apparatus was also confirmed upon genetic inhibition of autophagy in *ATG7*-silenced MM cells by immunoblotting (Fig. S6F). Also in this independent setting, we excluded autophagy inhibition to induce a UPR, by documenting no increase of total and spliced *XBPI*, *P4HB/PDI*, and *HSPA5/BiP* mRNA (Fig. S6G), further confirming that ER expansion stemmed from defective protein digestion, rather than from increased biogenesis. The data demonstrate a

Table 1. The interactome of SQSTM1 in basal conditions and under proteasome stress

Protein	Gene name	SQSTM1/Control ratio	Btz/UT ratio
sequestosome 1	<i>SQSTM1</i>	10.38	1
kelch-like ECH-associated protein 1	<i>KEAP1</i>	9.67	0.57
ependymin related 1	<i>EPDR1/UCC1</i>	9.19	0.68
glioblastoma amplified sequence	<i>GBAS</i>	8.71	0.25
insulin receptor	<i>INSR</i>	8.07	3.12
protein kinase C, iota	<i>PRKCI</i>	5.60	0.87
NOP2/Sun domain family, member 4	<i>NSUN4</i>	4.65	0.32
growth arrest-specific 6	<i>GAS6</i>	4.23	0.68
tripartite motif containing 21	<i>TRIM21</i>	3.62	1.91
NADH dehydrogenase (ubiquinone) Fe-S protein 2, 49kDa (NADH-coenzyme Q reductase)	<i>NDUFS2</i>	3.04	0.62
NADH dehydrogenase (ubiquinone) Fe-S protein 3, 30kDa (NADH-coenzyme Q reductase)	<i>NDUFS3</i>	2.82	0.51
G elongation factor, mitochondrial 2	<i>GFM2</i>	2.71	2.29
hydroxyacyl-CoA dehydrogenase/3-ketoacyl-CoA thiolase/enoyl-CoA hydratase (trifunctional protein), β subunit	<i>HADHB</i>	2.54	2.60
NADH dehydrogenase (ubiquinone) 1 α subcomplex, 5	<i>NDUFA5</i>	2.50	1.16
hydroxyacyl-CoA dehydrogenase/3-ketoacyl-CoA thiolase/enoyl-CoA hydratase (trifunctional protein), α subunit	<i>HADHA</i>	2.28	1.93
CD48 molecule	<i>CD48</i>	2.13	0.68
lactate dehydrogenase A	<i>LDHA</i>	2.09	1.57
reticulocalbin 2, EF-hand calcium binding domain	<i>RCN2</i>	2.08	1.09
ubiquitin	<i>UBC; UBB</i>	2.05	9.93

Specific SQSTM1 interactors with a SQSTM1/control ratio > 2. Bortezomib (Btz) / untreated (UT) ratios indicate relative interaction changes upon treatment.

selective negative control exerted by autophagy on the secretory pathway in MM cells, previously recognized only in normal PCs.²⁰ Interestingly, we found that Ig molecules did not accumulate upon lysosomal inhibition, indicating that misfolded Igs are recycled via the canonical proteasomal ER-associated degradation, at least in light chain-producing myeloma cells (Fig. S7; Table S2), confirming our previous findings in normal plasma cells.²⁰ Next, we confirmed that autophagy negatively regulates the ER in a panel of MM lines by revealing increased abundance of representative ER resident proteins upon pharmacological autophagic inhibition (Fig. 7B).

Having identified the ER as a major autophagic substrate in MM cells, we then hypothesized the saturated autophagic reserve identified in relatively PI-sensitive myelomas, as indicated by SQSTM1⁺ aggregates, to be associated with higher ER abundance. To test this hypothesis, we performed a proteomic and morphological comparison, respectively by SILAC LC-MS/MS and electron microscopy, of the MM lines containing respectively the highest and lowest number of SQSTM1⁺ puncta per cell, namely MM.1S and OPM2 cells. This combined approach revealed higher abundance of the ER in MM.1S cells (Fig. 7C-D; Dataset S2; Table S3). We confirmed this finding by immunoblotting analyses of representative ER proteins that were significantly more abundant in PI-sensitive than in PI-resistant MM lines (Fig. 7E).

By identifying the ER as the main cell compartment constitutively degraded by autophagy in MM cells, whose accumulation correlates with SQSTM1-containing aggregates, the data confirm that the autophagic capacity is saturated in inherently PI-sensitive myelomas.

Together, the data provide a more comprehensive and integrated picture of the cellular determinants of proteostasis and PI sensitivity in myeloma cells.

Discussion

The role of autophagy in cancer is multifaceted. In keeping with its cytoprotective action, loss-of-function mutations of genes encoding autophagic players have been linked with tumorigenesis, supporting the notion that autophagy is oncosuppressive in normal cells.^{22,27} The underlying mechanisms include the disposal of oncogenic proteins and damaged organelles, preventing local inflammation, necrosis, accumulation of reactive oxygen species, and oncogenic mutations.²⁸⁻³¹ Conversely, due to deregulated growth, cancer cells generally experience more stress (*e.g.*, hypoxia, nutrient deprivation, oxidative stress) and rely on adaptive strategies more than normal cells.^{32,33} Autophagy may thus be essential for transformed cells to resist metabolic, environmental, and pharmacological stress. Hence, autophagy inhibitors may be effective against cancer by killing tumor cells or sensitizing them to chemotherapy.²²

In addition, specific metabolic features could render certain tumors particularly dependent on autophagy. This applies to RAS-driven cancers, owing to impaired acetyl-CoA biosynthesis.²² Myeloma has been proposed to be particularly reliant on autophagy, due to its extraordinary UPS dependence, demonstrated by the successful clinical use of PIs,² owing, at least in part, to an imbalance between high proteasome workload, contributed by intensive Ig synthesis, and limited proteasome complement.^{5,34} Such imbalance is a general trait of Ig-producing PCs, which are also extremely PI-sensitive *in vitro*⁴ and *in vivo*.^{35,36} Long viewed as independent strategies with distinct substrates, the UPS and autophagy are now recognized as interdependent and complementary. Indeed, autophagy is activated in response to, and partially compensates for, proteasome impairment.^{15,23,24}

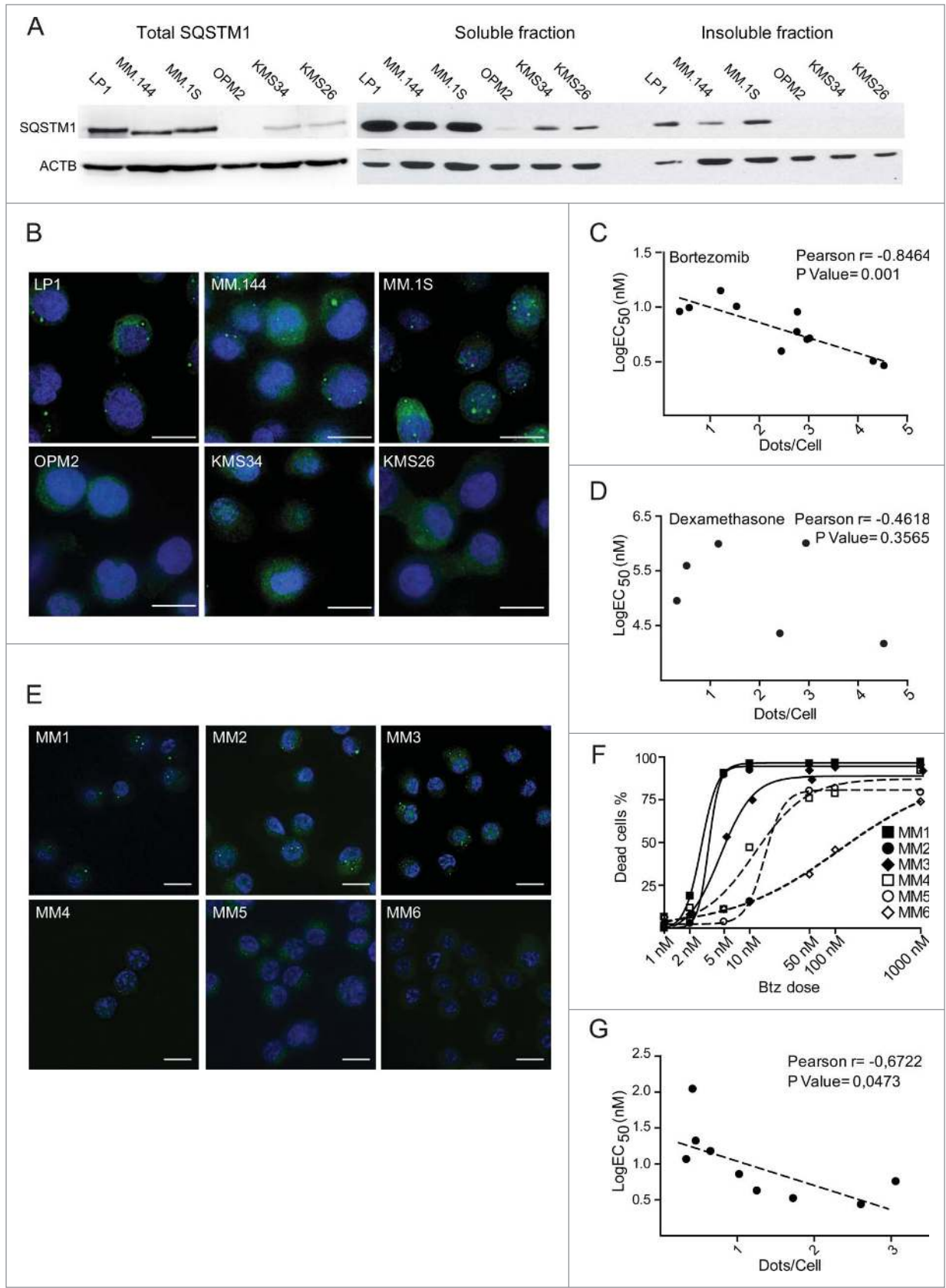


Figure 5. For figure legend, see page 1171.

The results presented herein are in keeping with previous reports supporting a protective role for basal autophagy in MM cell survival. However, pharmacological or genetic autophagic inhibition yielded discrepant results on PI sensitivity, ranging from synergy to antagonism.^{10,25,26,38,39} Notably, a phase 1 clinical trial showed that the combined use of bortezomib and HCQ for relapsed or refractory myeloma may improve therapeutic outcomes.⁴⁰ In our hands, autophagy inhibition with leupeptin or *SQSTM1* RNAi sensitized to bortezomib, and autophagy induction with rapamycin reduced PI sensitivity (Figs. 2 and 3), but HCQ and *ATG7* RNAi had no remarkable effects on PI toxicity (Figs. S1–S2). Such controversies might in part be accounted for by nonspecific effects achieved on additional signaling pathways, especially in the case of proximal autophagic inhibition.

Despite the general belief that autophagy inhibition should be beneficial against myeloma,^{10,11} we reasoned that our current poor understanding of the role of autophagy in this malignancy limits its therapeutic exploitation. Our recent discovery that long-lived plasma cells completely depend on autophagy²⁰ urged us to dissect the precise functions of autophagy in myeloma, to identify specific cargo-recognizing mechanisms, as a framework for novel markers and targets.

Autophagy serves a variety of cell-specific functions through selective target digestion via distinct receptor/adaptor proteins.⁴¹ We thus set out to test the role of the prototypical autophagic receptor, SQSTM1 in MM cells, assuming that a deeper knowledge of the molecular mechanisms of cargo selection may offer a framework to design more specific therapeutic agents.

Our work establishes SQSTM1 as an essential mediator of the cooperation between the UPS and autophagy in MM cells, providing a potential target to overcome PI resistance. First, we found that autophagy constitutively degrades aggregation-prone ubiquitinated proteins, as autophagy inhibition alone was sufficient to induce the accumulation of SQSTM1- and Ub-containing protein aggregates (Figs. 1 and S2). The relevance of SQSTM1-dependent autophagy as a functional reserve regulating PI susceptibility of MM cells is demonstrated by the documented capacity of autophagy inhibition or stimulation to respectively synergize or antagonize with the PI-induced build-up of ubiquitinated proteins and subsequent toxicity (Fig. 2). The coexistence of SQSTM1 aggregation and abundant autophagy in PI-sensitive myelomas in basal conditions suggests that certain tumors require more autophagic activity than they deploy. Indeed, an increased demand imposed by acute

proteasome stress is coped for by autophagy in PI-resistant MM cells, while aggravating accumulation of SQSTM1⁺ aggregates in PI-sensitive myelomas (Fig. 6). Taken together, our results yield proof-of-concept evidence in PI-sensitive myelomas of an insufficient autophagic reserve in the face of stresses that increase the functional demand for autophagy.

Moreover, we disclosed that MM cells adapt to proteasome stress via SQSTM1. We devised, for the first time, a wide-scope, quantitative LC-MS/MS analysis of proteins co-immunoprecipitated with endogenous SQSTM1 to define the interactome of SQSTM1 in steady conditions and under proteasome stress, using the SILAC technology to precisely quantify PI-induced changes. Together with immunofluorescence experiments, this powerful, unbiased approach led us to recognize the association of Ub-protein aggregates with SQSTM1 in myeloma cells. Moreover, we visualized aggregates nucleating into large, supra-metric bodies under PI treatment, and found a dramatic co-opting of SQSTM1 onto Ub-protein aggregates at the expense of other signaling partners. As a multi-domain adapter protein, SQSTM1 is a hub for multiple signaling pathways, including NF κ B and KEAP1-NFE2L2, along with its recognized role in autophagic cargo recognition.^{42,43} Our unbiased dynamic study of the SQSTM1 interactome revealed an intriguing adaptation of MM cells to proteasome stress, aimed to intensify the autophagic activity of this protein. Furthermore, we found that PIs not only divert SQSTM1 toward ubiquitinated proteins, but also selectively induce its de novo expression (Fig. 4). Together, these mechanisms define an unanticipated 2-fold adaptive plastic response to PIs, by which myeloma cells boost autophagic degradation of aggregates to compensate for UPS insufficiency. The data indicate that in MM cells autophagy and the UPS cooperate more closely than previously thought, as both constitutively degrade Ub-conjugated proteins, and provide insights into the nature and mechanisms of this cooperation. By furthering our understanding of the tight interplay between autophagy and the UPS,⁴⁴ these findings may help explain PI resistance and unveil new therapeutic targets. Indeed, the genetic ablation of SQSTM1 resulted in increased susceptibility to PIs and in vitro extinction of MM cell lines (Fig. 3).

Functional redundancy exists among autophagic receptors,¹⁷ as witnessed by the nonlethal mouse phenotype of systemic SQSTM1 deficiency,⁴⁵ and by the tissue-restricted and late-onset phenotype of Paget disease of bone, typically associated with germline inactivating mutations of the Ub-binding domain of

Figure 5 (See previous page). Spontaneous SQSTM1 aggregation specifically predicts bortezomib susceptibility in MM cell lines and in patient-purified myeloma cells. **(A)** Left panel: Immunoblot analysis of SQSTM1 on 1% SDS lysates from MM lines (representative blots, $n = 3$). Right panel: MM cells were lysed in 1% NP-40, insoluble material was resuspended in 1% SDS and the DNA was sonicated; equal protein amounts from NP-40 soluble and insoluble fractions were resolved by SDS-PAGE. Representative blots are shown ($n = 3$). **(B)** Immunofluorescence analysis of SQSTM1 accumulation in MM lines. Nuclei are stained blue with DAPI. Scale bar: 10 μ m. Representative images. **(C, D)** Linear Pearson's correlation between the average cellular counts of SQSTM1⁺ dots ($n \geq 80$ cells in ≥ 10 distinct fields) and the log EC₅₀ of bortezomib **(C)**, as assessed in Fig. S5, ($n = 11$) or that of dexamethasone **(D)**, as assessed upon 48 h treatment). **(E)** Immunofluorescence analysis of SQSTM1 accumulation in SD1/CD138⁺ cells purified from BM aspirates of 6 representative newly diagnosed MM patients. Nuclei are stained blue with DAPI. Scale bars: 10 μ m. **(F)** Apoptotic sensitivity to 24-h treatment with bortezomib was assessed in vitro by flow cytometry, as in Fig. S5 ($n = 9$). The panel shows 6 representative MM patients as in **(E)**. **(G)** Linear Pearson's correlation between the average cellular counts of SQSTM1⁺ dots in each patient and the log EC₅₀ of bortezomib ($n = 9$ patients).

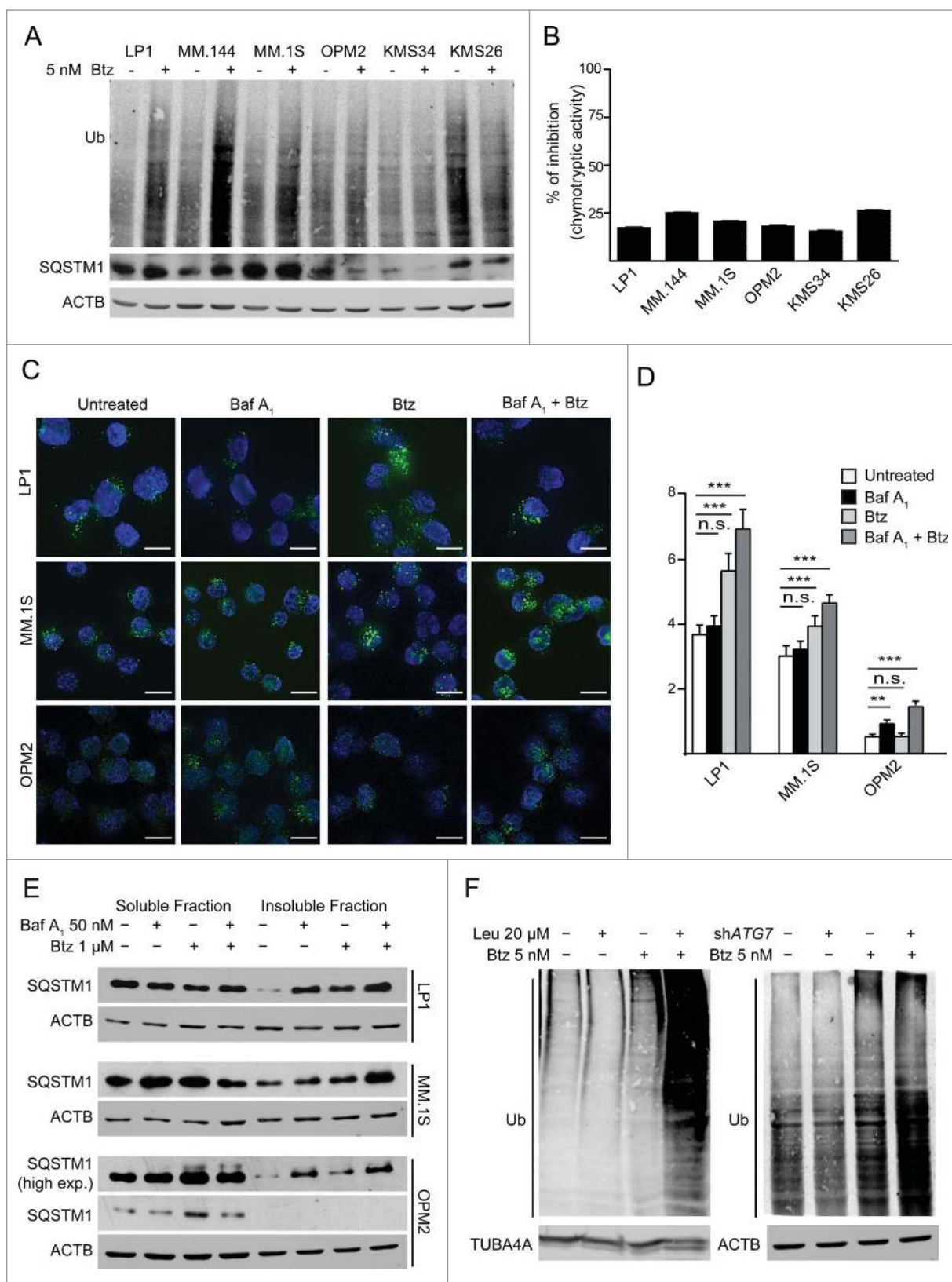


Figure 6. For figure legend, see page 1173.

SQSTM1.⁴⁶ Thus, the absolute requirement of SQSTM1 for MM cell survival offers a specific therapeutic target, and a framework for identifying additional new targets.

Further supporting specificity, while SQSTM1 is protective to MM cells, it demonstrates toxicity in distinct models, possibly via hampered proteasomal degradation of substrates sequestered into insoluble aggregates.⁴⁷ In mice with liver-specific ablation of autophagy, *SQSTM1* silencing prevents protein aggregation, oxidative stress, and tissue hypertrophy.⁴⁸ Such toxicity of SQSTM1 was suppressed by *NFE2L2* ablation, suggesting that the otherwise protective SQSTM1-KEAP1-NFE2L2 axis may turn maladaptive in certain conditions.⁴⁹ The addiction of MM cells to SQSTM1-dependent autophagy for survival, identified herein, may reflect the fragile proteostasis of malignant PCs, already challenged in the absence of exogenous stressors, with overloaded UPS, high PI vulnerability, and intense autophagy.¹² Accordingly, we found that SQSTM1 silencing was extremely toxic for MM cell lines, but not for B lymphomas, and that its knockdown specifically sensitized MM cells to the first-in-class PI bortezomib, but not to other anti-myeloma agents (Fig. 3). The mechanisms whereby insufficient SQSTM1-dependent autophagy is toxic to MM cells remain to be elucidated. A recent report of BIK-mediated apoptosis triggered by SQSTM1 downregulation upon autophagy induction suggests a possible mechanism.⁵⁰

Through unbiased analyses of cells in which autophagy had been blocked pharmacologically or genetically, our work disclosed that in MM cells autophagy not only disposes of aggregation-prone ubiquitinated proteins, but also constitutively restricts the secretory compartment, a previously unrecognized function in MM cells (Fig. 7). Both activities are predicted to reduce the UPS workload.^{2,12} The data extend our previous finding that autophagy moderates ER expansion in normal differentiating PCs to their malignant counterparts.²⁰

The present study provides a more comprehensive understanding of protein degradation in MM cells. In view of the tight and multifaceted cooperation, documented herein, between autophagy and the UPS, the data encourage us to integrate the model currently proposed to underlie PI sensitivity, which exclusively refers to the proteasomal workload and capacity,⁵ so as to include autophagy in the functional assessment of MM cell biology. The peculiar feature of being induced by PIs and specifically digested by autophagy renders SQSTM1 an integrated reporter of stress in both proteocatabolic routes, possibly indicative of

high susceptibility of myeloma cells to negative proteostasis regulators, and particularly PIs. Indeed, we found that the presence of SQSTM1⁺ aggregates, as assessed biochemically or by immunofluorescence, neatly discriminated between 2 groups of MM lines or patients, characterized by differential inherent vulnerability to PIs (Fig. 5). This striking correlation urges us to test SQSTM1 as a potential, highly needed single-cell prognostic tool to predict individual clinical responses to PI treatment. The circumstance that both the abundance and cellular distribution of SQSTM1 change under proteasome stress is likely to magnify its accuracy as a reporter. Should this marker be able to predict the clinical responsiveness to PIs, at least in selected groups of patients, a new tool could be developed for clinical hematologists to help inform the design of personalized therapeutic regimens.

Materials and Methods

Cell cultures

Human myeloma cell lines (kindly provided by Giovanni Tonon, San Raffaele Scientific Institute, Milan, Italy) and B lymphoma cell lines (kindly provided by Paolo Ghia, San Raffaele Scientific Institute, Milan, Italy) were cultured in RPMI medium (Gibco-Life Technologies, 31860) supplemented with 10% fetal bovine serum (Euroclone, ECS0180L), L-glutamine (2 mM; Gibco-Life Technologies, 25030-081), penicillin/streptomycin (100 µg/ml; Lonza, 17-602E) and sodium pyruvate (1 mM; Sigma-Aldrich, S8636). Each culture was examined for Ig secretion and SDC1/CD138 expression, and periodically tested for mycoplasma negativity. All lines are routinely genotyped by the Tonon lab using 2 protocols, one based on a set of a microsatellite markers set in collaboration with the Mayo Clinic (Scottsdale, AZ), and a second one, based on short tandem repeats assessment, as developed by the DSMZ (details at <http://www.dsmz.de/services/services-human-and-animal-cell-lines/online-str-analysis.html>).

Patient-derived MM cells were purified from BM aspirates by SDC1 immunomagnetic-positive selection using the Human Plasma Cell Isolation kit (Miltenyi Biotech, 130-093-628). Informed consent was obtained in accordance with the declaration of Helsinki. Approval for use of primary samples was obtained from the Institutional Review Board of the San Raffaele Scientific Institute. Cells were treated with leupeptin,

Figure 6 (See previous page). A proteostatic autophagic reserve is saturated in PI-sensitive myelomas. **(A)** Immunoblotting analysis of the effect of 8-h treatment with low dose (5 nM) bortezomib (Btz) on the accumulation of ubiquitinated proteins in the indicated panel of MM lines (representative blot, $n = 3$). **(B)** The level of proteasome inhibition achieved in **(A)** was assayed in the indicated MM lines by means of a fluorogenic peptide specifically cleaved by the proteasomal chymotryptic peptidase activity (% inhibition in one representative experiment). **(C–E)** Differential capacity of PI-sensitive and -resistant MM cells to deploy autophagy against pharmacological proteasome stress. **(C)** Immunofluorescence analysis of SQSTM1 accumulation in MM lines treated with 1 µM bortezomib (Btz) and 50 nM bafilomycin A₁ (Baf A1), alone or in combination, for 1 h. Nuclei are stained blue with DAPI. Scale bar: 10 µm. Representative images. **(D)** Average cellular counts of SQSTM1⁺ puncta in the experiment shown in panel **(C)** (average \pm s.e.m., $n \geq 80$ cells in 7 distinct fields). * $P < 0.05$; ** $P < 0.01$; *** $P < 0.001$ by unpaired Student t test. **(E)** Immunoblot analysis of SQSTM1 protein abundance in the NP-40 soluble and insoluble cellular fraction (as in Fig. 5A) of the indicated MM lines treated as in panel **(C)**. Equal protein amounts were resolved by SDS-PAGE. Representative blots are shown ($n = 3$). **(F)** Immunoblot analysis of polyubiquitinated proteins in OPM2 cells subjected to the indicated proteasome inhibition for 24 h, alone or combined with pharmacological (20 µM leupeptin, left panel) or genetic (lentiviral *ATG7* RNAi as in Fig. S1) inhibition of autophagy (representative blots, $n = 3$).

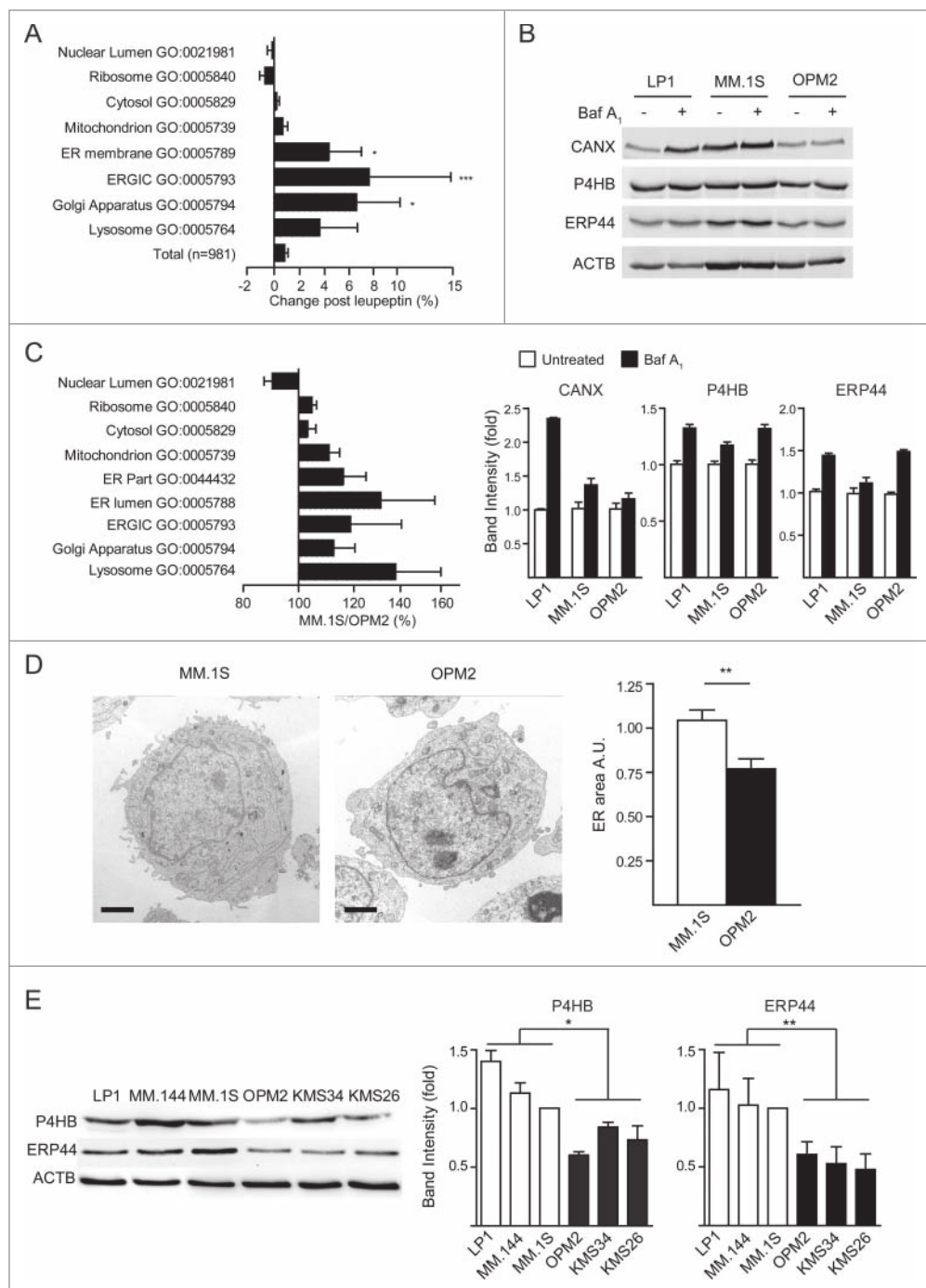


Figure 7. Endoplasmic reticulum is the main cell compartment degraded by autophagy in MM cells. **(A)** Proteome changes upon autophagy inhibition (as in **Fig. S4**) by SILAC LC-MS/MS. The 981 proteins quantified in 2 independent experiments were grouped by the indicated gene ontology (GO) categories (average ratios \pm s.e.m.; significance calculated against all quantified proteins). **(B)** Immunoblot analysis of selected ER proteins in MM cells treated with 100 nM bafilomycin A₁ (Baf A₁) for 24 h (representative image, $n = 4$). Top, representative blots; bottom, quantification normalized by ACTB/actin expressed relative to untreated cells (average \pm s.e.m., $n = 4$). **(C)** Relative protein abundance in MM.1S vs. OPM2 cells by SILAC. The relative abundance of 1,674 proteins was quantified in 2 independent experiments. Proteins were assigned to the corresponding GO cell compartment (average GO values \pm s.e.m.). **(D)** ER morphology was assessed in OPM2 and MM.1S by electron microscopy and the area of the cell occupied by the ER was quantified by stereology. Left, representative images; right, quantification (average \pm s.e.m.; $n \geq 30$ cells per line). Scale bar: 1 μ m. **(E)** Selected ER proteins were quantified in MM lines by immunoblot analysis. Left, representative blots ($n = 4$ independent experiments). Right, average quantification \pm s.e.m. * $P < 0.05$; ** $P < 0.01$; *** $P < 0.001$ by unpaired Student *t* test.

SDC1 APC conjugated antibody (Ab) (Miltenyi Biotec, 130–091–250). Data were obtained with Accuri C6 Flow Cytometer (BD biosciences, San Jose, CA) and analyzed using the FCS Express 4 Flow Research Edition (De Novo Software). Patient-derived MM

cells were seeded at 30,000 cells/well and treated for 24 h as indicated.

bafilomycin A₁, chloroquine, rapamycin, hydroxychloroquine (Sigma-Aldrich, L2884, B1793, C6628, R8781, H0915) or bortezomib (Millennium, VELCADE™) as indicated.

Flow cytometric analyses of cell viability

Cells were treated as indicated, harvested and stained with fluorescein isothiocyanate or allophycocyanin (APC)-conjugated ANXA5/annexinV (BD PharmMingen, 556547, 550474) and propidium iodide, as per the manufacturer's instructions. SDC1 positivity was controlled with anti-human

cells were seeded at 30,000 cells/well and treated for 24 h as indicated.

Lentiviral RNA interference

Plasmid constructs expressing anti-*ATG7*, anti-*SQSTM1*, and control shRNAs were obtained with Mission shRNAs pLKO.1-puro (nontarget shRNA: SHC002; sh*ATG7* 1: TRCN0000007584; sh*ATG7* 2: TRCN0000007587; sh*SQSTM1* 1: TRCN0000007234; sh*SQSTM1* 2: TRCN0000007236; Sigma-Aldrich). Lentiviral vectors were packaged with Sigma-

Aldrich Mission shRNAs, pMD2-VSV-G, pMDLg/pRRE and pRSV-Rev plasmids in HEK 293T cells for 14 h, then medium was replaced and 1 mM Na-butyrate added. 48 h later cell supernatant fractions were collected, ultracentrifuged, filtered and administered to MM cells with polybrene (8 µg/ml; Sigma-Aldrich AL-118) for 16 h. Transduced cells were selected for 1 wk with 2 µg/ml puromycin (Sigma-Aldrich, P9620).

To assess shRNA toxicity, the gene encoding puromycin resistance was replaced with GFP. The GFP-positive proportion of viable cells for each shRNA was determined 3 d after infection and then monitored by Accuri C6 Flow Cytometer (BD Biosciences, San Jose CA) upon staining with APC-conjugated ANXA5 (BD PharmMingen, 550474) and propidium iodide, and normalized to initial values and nonspecific toxicity.

shRNA sequences. shATG7(1): CCGGGCCTGCTGAG-GAGCTCTCCATCTCGAGATGGAGAGCTCCTCAGCAG-GCTTTTTT; shATG7(2): CCGGCCAGCTATTGGAACAC-TGTAICTGAGTACAGTGTCCAATAGCTGGGTTTTT; shSQSTM1 (1): CCGGCGAGGAATTGACAATGGCCATC-TCGAGATGGCCATTGTCAATTCCTCGTTTTT; shSQSTM1 (2): CCGGCCGAATCTACATTAAGAGAAGACTCGAG-TTCTCTTTAATGTAGATTCGGTTTTT.

Colony-forming assay

Cells were resuspended in RPMI complete medium with 0.4% 2-hydroxyethylagarose (Sigma-Aldrich, A9414) at a concentration of 5,000 cells/well and plated over a 0.8% agar layer in a 6-well plate. The experiment was performed in duplicate and plates were incubated at 37°C in a humidified incubator for 21 d. Upon staining with thiazolyl blue tetrazolium bromide (Sigma-Aldrich, M2128) diluted 1:10 in 1X phosphate-buffered saline (PBS; Euroclone, ECB4004L) for 4 h, colonies containing at least 20 cells as assessed by light microscopy were counted.

Immunoblot analyses

Total cellular extracts were obtained by lysis in 150 mM NaCl, 10 mM Tris-HCl (pH 7.5), 1% SDS (Sigma-Aldrich, 05030) for 15 min on ice. Genomic DNA was sheared by 30 min sonication.

To obtain soluble fractions, cells were collected and lysed in 150 mM NaCl, 10 mM Tris-HCl (pH 7.5) and 1% Nonidet NP-40 substitute (Sigma-Aldrich, IGEPAL CA-630, I8896), supplemented with protease inhibitors (30 µg; Roche, 05056489001), for 15 min on ice. Insoluble material was pelleted by centrifugation at 16,000 g for 15 min at 4°C and resuspended in 150 mM NaCl, 10 mM Tris-HCl (pH 7.5), 2% SDS (Sigma-Aldrich, 05030). After lysis, proteins were quantified by BCA assay. Proteins (30 µg) were resolved by 8%, 10%, 12% or 15% SDS-PAGE and blotted on nitrocellulose membrane (Bio-Rad, 162–0115). Membranes were blocked in 5% milk in PBS, 0.1% Tween-20 (Sigma-Aldrich, 274348), incubated with primary and secondary antibodies, thoroughly washed with PBS, 0.1% Tween-20, and proteins revealed by ECL using a Chemi-Doc-it (UVP) for HRP-conjugated secondary Ab or at FLA9000 (FujiFilm, Tokyo Japan) for Alexa Fluor conjugated secondary antibodies (Life Technologies, A-21235, A-21036, A-21244,

A-21450). Band densitometric analysis was performed with ImageJ free software (<http://rsbweb.nih.gov/ij/>). The following Abs were used: guinea pig anti-SQSTM1 C-terminal polyclonal Ab (1:1000 dilution; ProGen, GP62-C); rabbit anti-SQSTM1 (1:1000; Sigma-Aldrich, P0067); rabbit anti-MAP1LC3 polyclonal Ab (1:500; Novus Biologicals, NB100–220); rabbit anti-ATG7 (1:1000; Sigma-Aldrich, A2856); anti-ACTB/β actin (1:2000; Sigma-Aldrich, A5441); mouse anti-TUBA4A/α tubulin (1:5000; Sigma-Aldrich, T6074); rabbit anti-P4HB (1:1000, polyclonal antibody; kind gift of Ineke Braakman, Utrecht, NL); goat anti-KEAP1 (1:200; Santa Cruz Biotechnologies, sc-15246); mouse anti-ERP44 (1:1000; monoclonal Ab (36C9), kind gift of Roberto Sitia, Milano, Italy); rabbit anti-PRDX4 (1:1000; AbFrontier, PA0009); mouse anti-Ub monoclonal Ab (P4D1; 1:500; Santa Cruz Biotechnology, sc-8017).

SQSTM1 immunoprecipitation

Cells were collected and lysed in 150 mM NaCl, 10 mM Tris-HCl (pH 7.5), 1% Nonidet NP-40 substitute, supplemented with protease inhibitors, incubated for 15 min on ice; the nuclei were then pelleted at 1000 g for 15 min. Soluble material was quantified and 10 mg protein lysate incubated for 2 pre-clearing cycles with 30 µl protein A Sepharose fast flow beads (GE Healthcare, 17–0618–01) for 3 h. Pre-cleared lysate was incubated for 16 h with 30 µg beads pre-conjugated with 5 µg rabbit anti-SQSTM1 antiserum (Sigma-Aldrich, PA0067) or control serum. Beads were washed 4 times in 150 mM NaCl, 10 mM Tris-HCl (pH 7.5), 0.1% Nonidet NP-40 substitute, and resuspended in Laemmli buffer for SDS-PAGE resolution.

Immunofluorescence

MM cells were seeded on poly-L-lysine-coated slides, fixed with 4% paraformaldehyde, and permeabilized with PBS 0.1% Triton X-100. Cells were stained with guinea pig SQSTM1 antiserum (1:200), C-terminal (Progen, GP62-C), rinsed in PBS, and stained with Alexa Fluor 488 goat anti-guinea pig IgG (1:500; Life Technologies, A11073) and Hoechst 33,342 (Life Technologies, H3570). Images were acquired with Deltavision (Applied Precision, Issaquah, WA) with an Olympus 60× objective with a numerical aperture of 1.42. For every sample several stacks were acquired on the z-axis. Images were deconvoluted using SoftWorks 3.5.0 (Applied Precision) and processed with ImageJ. More than 80 cells per sample were counted and analyzed.

Intracellular ATP quantification

ATP was quantified with the luminescent CellTiter-Glo assay per the manufacturer's instructions (Promega, G7570), as described.²⁰ Briefly, for each condition 10,000 living cells were plated in quadruplicate on white 96-well multiwell plates and were analyzed with a Victor plate reader (Perkin-Elmer, Waltham MA).

Proteasome activity assays

Proteasome activity was determined using fluorogenic peptides, as previously described.^{5,6} Briefly, cells were sonicated in ice-cold buffer (50 mM Tris-HCl [pH 7.5], 1 mM DTT, 0.25 M sucrose, 5 mM MgCl₂, 0.5 mM EDTA, 2 mM ATP), and

extracts were prepared by centrifugation (30 min 10,000 g, and 15 min 100,000 g). Proteasome-specific chymotryptic peptidase activity was assayed by monitoring the production of 7-amino-4-methylcoumarin (amc) from 100 μ M Suc-LLVY-amc (Bachem, I-1395) in 20 mM Tris-HCl (pH 7.5), 1 mM ATP, 2 mM MgCl₂, 0.2% bovine serum albumin. Reactions were started by adding an aliquot of cell extract, and the fluorescence of released amc (excitation, 380 nm; emission, 460 nm) was monitored continuously at 37°C with a Carry Eclipse spectrofluorometer (Varian, Palo Alto, CA). Background activity (due to nonproteasomal degradation) was determined by addition of 10 μ M MG132 (Sigma-Aldrich C2211). Assays were calibrated using standard free fluorophore solutions, and reaction velocities calculated from the slopes of the initial linear curve portions. Substrate consumption at the end of incubation never exceeded 1%.

Electron microscopy

Cells were pelleted and processed as described.²⁰ Ultrathin sections were observed with a Zeiss Leo 912AB electron microscope (Zeiss, Oberkochen Germany) operating at 80 kV. Digital micrographs were captured with a 2kx2k Proscan slow-scan charge-coupled device camera system (Proscan HSC2, Lagerlefeld Germany) controlled by the integrated Soft Imaging software (Soft Imaging Software). ER was measured by stereography with a fixed grid in ImageJ.

qRT-PCR

For RT-PCR, RNA was extracted from 1×10^6 cells with Trizol (Invitrogen, 10296028), 1000 ng RNA retrotranscribed with ImProm-II Reverse Transcriptase (Promega, A3800), and cDNA corresponding to 2–5 ng of original RNA used as template in qPCR reactions.

qPCR were performed in 10 μ L mix with 5 μ L SYBR green I master mix (Roche, 04707516001) on Roche LightCycler 480 and 1 μ L 5 μ M primers. Data were analyzed on Roche LC480 software with Advance Relative Quantification. Human H3 expression was used as normalizer in the analyses. Primers used were: *hATG7* FW: AGACAGAGGGCAGGATAGCA; *hATG7* RV: TGGAACAAGCAGCAAATGAG; *hHSPA5* FW: TAGCGTATGGTGTGCTGCTGTC; *hHSPA5* RV: TGACA CCTCCACAGTTTCA; *hP4HBF* FW: TCACATCCTGCTG TTCTTGC; *hP4HB* RV: GTCGCTGTCGATGAAGATGA; *hSQSTM1* FW: GGGGCGCCCTGAGGAACAGA; *hSQSTM1* RV: CCTGGTGAGCCAGCCGCCTT; *hXBP1s* FW: CC GCAGCAGGTGCAGG; *hXBP1s* RV: GAGTCAATACCGC-CAGAATCCA; *hXBP1* total FW: GCAAGCGACAGCGCCT; *hXBP1* total RV: TTTTCAGTTTCTCCTCAGCG; *hH3* FW: GTGAAGAAACCTCATCGTTACAGGCCTGGT; *hH3* RV: CTGCAAAGCACCAATAGCTGCACTCTGGAA; *hNBR1* FW: GCGAGCTGAGAAGAAACAACG; *hNBR1* RV: GAAGGTGAGTCCCATCAGGC; *hOPTN* FW: TTCGGC CTGGACAGAGAAAC; *hOPTN* RV: TGCCTTCTCTGC TTGTAGCC.

SILAC mass-spectrometry

MM lines were grown in complete SILAC RPMI medium (Thermo Scientific, 89984) supplemented with “light” (Lys0, Arg0), “heavy” (Lys8, Arg10) or “intermediate” (Lys4, Arg6) SILAC amino acids (arginine, Sigma-Aldrich, 643440, 608033; lysine, Cambridge Isotope Laboratories, DLM-2640, CNLM-291) for 14 d, with 95% mean labeling efficiency. Lysates were loaded in SDS-PAGE, trypsin-digested, and analyzed using a LTQ-Orbitrap mass spectrometer (Thermo Fisher Scientific, Waltham MA). For SILAC analyses of leupeptin effects, OPM2 cells were treated for 24 h with 20 μ M leupeptin. Treated and untreated cells differentially labeled were mixed 1:1 and lysed in 150 mM NaCl, 10 mM Tris-HCl (pH 7.5), 1% SDS for 15 min on ice. Samples were loaded on a 10% SDS-PAGE gel and stained with colloidal Coomassie brilliant blue. Gel slices were excised from the gel sampling the entire length of the lanes from the direct and reverse experiments (12 slices each). For MM.1S and OPM2 comparative analysis, differentially labeled cells were mixed 1:1 and a cellular fractionation was performed using the Qproteome Cell Compartment Kit (Qiagen, 37502). Cytosolic, membrane and nuclear fractions were loaded on a 10% SDS-PAGE gel and 10 gel slices were excised from each lane from the direct and reverse experiments. For SQSTM1 dynamic interactome SILAC, MM.1S cells were labeled with “light,” “intermediate,” and “heavy” amino acids and IP performed as described in Figure S2. Immunoprecipitates were mixed 1:1:1 and loaded on a 10% SDS-PAGE gel and 10 gel slices were excised and analyzed by LC-MS/MS. After reduction with 10 mM DTT (Sigma-Aldrich, D9779), alkylation with 55 mM iodoacetamide (Sigma-Aldrich, I1149) and overnight tryptic digestion, digests were desalted and concentrated on C18 Stage Tips (Proxeon Biosystems, SP301) and then separated on a NanoLC (EasyLC, Proxeon Biosystems, Odense Denmark). Peptide separation occurred on a RP homemade 15-cm reverse phase (RP) spraying fused silica capillary column (75 μ m i.d.), packed inhouse with 3- μ m ReproSil-Pur 120 C18-AQ (Dr. Maisch GmbH, Germany). A gradient of eluents A (H₂O with 2% v/v ACN, 0.5% v/v acetic acid) and B (80%ACN with 0.5% v/v acetic acid) was used to achieve separation, from 7% B (at 0 min 0.2 μ L/min flow rate) to 40% B (in 70 min, 0.2 μ L/min flow rate). The LC system was connected to an LTQ-Orbitrap mass spectrometer (Thermo Fisher Scientific, Waltham MA) equipped with a nanoelectrospray ion source (Proxeon Biosystems, Odense, Denmark). MS and MS/MS spectra were acquired selecting the 10 most intense ions per survey spectrum acquired in the orbitrap from *m/z* 300–1750 with 30,000 resolution. Target ions selected for the MS/MS were fragmented in the ion trap and dynamically excluded for 60s. For accurate mass measurements, the lock-mass option was employed. Technical replicates were conducted on the LC-MS/MS part of the analysis. Raw data were processed with MaxQuant (version 1.2.2.5) and peptides identified from MS/MS spectra against the Human Uniprot Complete Proteome Set database (ver. 2012_05) using the Andromeda search engine. Cysteine carbamidomethylation was used as fixed modification, methionine oxidation and protein N-terminal acetylation as

variable modifications. Mass deviation for MS/MS peaks was set at 0.5 m/z units with a maximum of 2 missed cleavages allowed. The peptides and protein false discovery rates were set to 0.01; the minimal length required for a peptide was 6 amino acids; minimum 2 peptides and at least one unique peptide were required for high-confidence protein identification; for quantitative analysis options Re-quantify and second peptide were selected. The lists of identified proteins were filtered to eliminate reverse hits and known contaminants.

Statistical and data analyses

For mass spectrometry, the Perseus software (v.1.1.1.21) was used. Identification of significant protein changes required: *i*) significance B at $P < 0.05$; *ii*) ratio normalized values concordant in both direct and reverse experiments; *iii*) ≥ 2 ratio counts. Proteins consistently upregulated were run through functional annotation clustering on DAVID web resource, as described.^{20,51} For general analyses of graphs and data, the Prism software, version 4.0 (GraphPad) was used. Statistical significance was tested with a 2-tailed Student *t* test ($\alpha = 0.05$). Figures were assembled with Adobe Illustrator.

Disclosure of Potential Conflicts of Interest

No potential conflicts of interest were disclosed.

References

- Goldberg AL. Development of proteasome inhibitors as research tools and cancer drugs. *J. Cell Biol.* 2012; 199:583-8; PMID:23148232; <http://dx.doi.org/10.1083/jcb.201210077>
- Hideshima T, Anderson KC. Biologic impact of proteasome inhibition in multiple myeloma cells from the aspects of preclinical studies. *Semin. Hematol.* 2012; 49: 223-27; PMID:22726545; <http://dx.doi.org/10.1053/j.seminhematol.2012.04.006>
- Shah JJ, Orłowski RZ. Proteasome inhibitors in the treatment of multiple myeloma. *Leukemia* 2009; 23:1964-79; PMID:19741722; <http://dx.doi.org/10.1038/leu.2009.173>
- Cenci S, Mezghrani A, Cascio P, Bianchi G, Cerruti F, Fra A, Lelouard H, Masciarelli S, Mattioli L, Oliva L *et al*. Progressively impaired proteasomal capacity during terminal plasma cell differentiation. *EMBO J.* 2006; 25:1104-13; PMID:16498407; <http://dx.doi.org/10.1038/sj.emboj.7601009>
- Bianchi G, Oliva L, Cascio P, Pengo N, Fontana F, Cerruti F, Orsi A, Pasqualetto E, Mezghrani A, Calbi V, *et al*. The proteasome load versus capacity balance determines apoptotic sensitivity of multiple myeloma cells to proteasome inhibition. *Blood* 2009; 113:3040-49; PMID:19164601; <http://dx.doi.org/10.1182/blood-2008-08-172734>
- Cenci S, Oliva L, Cerruti F, Milan E, Bianchi G, Raule M, Mezghrani A, Pasqualetto E, Sitia R, Cascio P. Pivotal Advance: Protein synthesis modulates responsiveness of differentiating and malignant plasma cells to proteasome inhibitors. *J. Leukoc Biol.* 2012; 92:921-31; PMID:22685320; <http://dx.doi.org/10.1189/jlb.1011497>
- Richardson PG, Barlogie B, Berenson J, Singhal S, Jagannath S, Irwin DH, Rajkumar SV, Srkalovic G, Alsina M, Anderson KC. Extended follow-up of a phase II trial in relapsed, refractory multiple myeloma: final time-to-event results from the SUMMIT trial. *Cancer* 2006; 106:1316-19; PMID:16470606; <http://dx.doi.org/10.1002/cncr.21740>
- Richardson PG, Sonneveld P, Schuster M, Irwin D, Stadtmauer E, Facon T, Harousseau JL, Ben-Yehuda D, Lonial S, Goldschmidt H, *et al*. Extended follow-up of a phase 3 trial in relapsed multiple myeloma: final time-to-event results of the APEX trial. *Blood* 2007; 110:3557-60; PMID:17690257; <http://dx.doi.org/10.1182/blood-2006-08-036947>
- Vij R, Wang M, Kaufman JL, Lonial S, Jakubowiak AJ, Stewart AK, Kukreti V, Jagannath S, McDonagh KT, Alsina M, *et al*. An open-label, single-arm, phase 2 (PX-171-004) study of single-agent carfilzomib in bortezomib-naïve patients with relapsed and/or refractory multiple myeloma. *Blood* 2012; 119:5661-70; PMID:22555973; <http://dx.doi.org/10.1182/blood-2012-03-414359>
- Hideshima T, Richardson PG, Anderson KC. Mechanism of action of proteasome inhibitors and deacetylase inhibitors and the biological basis of synergy in multiple myeloma. *Mol. Cancer Ther.* 2011; 10:2034-42; PMID:22072815; <http://dx.doi.org/10.1158/1535-7163.MCT-11-0433>
- Aronson LI, Davies FE, Dang ER. protein overload. Targeting protein degradation to treat myeloma. *Haematologica* 2012; 97:1119-30; PMID:22580998; <http://dx.doi.org/10.3324/haematol.2012.064923>
- Cenci S. The proteasome in terminal plasma cell differentiation. *Semin Hematol.* 2012; 49:215-22; PMID:22726544; <http://dx.doi.org/10.1053/j.seminhematol.2012.04.005>
- Lum JJ, DeBerardinis RJ, Thompson CB. Autophagy in metazoans: cell survival in the land of plenty. *Nat. Rev. Mol. Cell Biol.* 2005; 6:439-48; PMID:15928708; <http://dx.doi.org/10.1038/nrm1660>
- He C, Klionsky DJ. Regulation mechanisms and signaling pathways of autophagy. *Annu. Rev. Genet.* 2009; 43: 67-93; PMID:19653858; <http://dx.doi.org/10.1146/annurev-genet-102808-114910>
- Mizushima N, Komatsu M. Autophagy: renovation of cells and tissues. *Cell* 2011; 147:728-41; PMID:22078875; <http://dx.doi.org/10.1016/j.cell.2011.10.026>
- Kroemer G, Marino G, Levine B. Autophagy and the integrated stress response. *Mol. Cell* 2010; 40:280-93; PMID:20965422; <http://dx.doi.org/10.1016/j.molcel.2010.09.023>
- Johansen T, Lamark T. Selective autophagy mediated by autophagic adapter proteins. *Autophagy* 2011; 7:279-96; PMID:21189453; <http://dx.doi.org/10.4161/auto.7.3.14487>
- McLeod IX, Jia W, He YW. The contribution of autophagy to lymphocyte survival and homeostasis. *Immunol. Rev.* 2012; 2:195-204; <http://dx.doi.org/10.1111/j.1600-065X.2012.01143.x>
- Deretic V, Saitoh T, Akira S. Autophagy in infection, inflammation and immunity. *Nat. Rev. Immunol.* 2013; 13:722-37; PMID:24064518; <http://dx.doi.org/10.1038/nri3532>
- Pengo N, Scolari M, Oliva L, Milan E, Mainoldi F, Raimondi A, Fagioli C, Merlini A, Mariani E, Pasqualetto E, *et al*. Plasma cells require autophagy for sustainable immunoglobulin production. *Nat. Immunol.* 2013; 14:298-305; PMID:23354484; <http://dx.doi.org/10.1038/ni.2524>
- Conway KL, Kuballa P, Khor B, Zhang M, Shi HN, Virgin HW, Xavier RJ. ATG5 regulates plasma cell differentiation. *Autophagy* 2013; 9:528-37; PMID:23327930; <http://dx.doi.org/10.4161/auto.23484>
- White, E. Deconvoluting the context-dependent role for autophagy in cancer. *Nat. Rev. Cancer* 2012; 12:401-10; PMID:22534666; <http://dx.doi.org/10.1038/nrc3262>
- Pandey UB, Nie Z, Batlevy Y, McCray BA, Ritson GP, Nedelsky NB, Schwartz SL, DiProspero NA, Knight MA, Schuldiner O, *et al*. HDAC6 rescues neurodegeneration and provides an essential link between autophagy and the UPS. *Nature* 2007; 447:859-63; PMID:17568747; <http://dx.doi.org/10.1038/nature05853>
- Choi AM, Ryter SW, Levine B. Autophagy in human health and disease. *N. Engl. J. Med.* 2013; 368:651-62; PMID:23406030; <http://dx.doi.org/10.1056/NEJMra1205406>

Acknowledgements

We thank Federica Loro for patient assistance, and all the Cenci lab members for creative discussions. We are particularly grateful to: Annapaola Andolfo, Holger W. Auner, Elisa Benatti, Stefano Casola, Angela Cattaneo, Floriana Cremasco, Paolo Dellabona, Monica Fabbri, Francesca Fontana, Luigi Gennari, Fernando Gianfrancesco, Luigi Maiuri, Giampaolo Merlini, Daniela Merlotti, Andrea Orsi, Niccolò Pengo, Maurizio Ponzoni, Fulvio Reggiori, Umberto Restuccia, Carmine Settembre, Roberto Sitia, and Giovanni Tonon.

Funding

The work was supported by grants to S.C. from the Multiple Myeloma Research Foundation (Senior Research Award 2010), the Italian Ministry of Health (Giovani Ricercatori 1143560) and the Italian Association for Cancer Research (AIRC, Investigator Grant 14691 and Special Program Molecular Clinical Oncology 5 per mille n. 9965).

Supplemental Material

Supplemental data for this article can be accessed on the publisher's website.

25. Hoang B, Benavides A, Shi Y, Frost P, Lichtenstein A. Effect of autophagy on multiple myeloma cell viability. *Mol. Cancer Ther.* 2009; 8:1974-84; PMID:19509276; <http://dx.doi.org/10.1158/1535-7163.MCT-08-1177>
26. Lamy L, Ngo VN, Emre NCT, Shaffer 3rd AL, Yang Y, Tian E, Nair V, Kruhlak MJ, Zingone A, Landgren O, et al. Control of autophagic cell death by caspase-10 in multiple myeloma. *Cancer Cell* 2013; 23:435-49; PMID:23541952; <http://dx.doi.org/10.1016/j.ccr.2013.02.017>
27. Levine B, Kroemer G. Autophagy in the pathogenesis of disease. *Cell* 2008; 132:27-42; PMID:18191218; <http://dx.doi.org/10.1016/j.cell.2007.12.018>
28. Mathew R, Kongara S, Beaudoin B, Karp CM, Bray K, Degenhardt K, Chen G, Jin S, White E. Autophagy suppresses tumor progression by limiting chromosomal instability. *Genes Dev.* 2007; 21:1367-81; PMID:17510285; <http://dx.doi.org/10.1101/gad.1545107>
29. Degenhardt K, Mathew R, Beaudoin B, Bray K, Anderson D, Chen G, Mukherjee C, Shi Y, Gélinas C, Fan Y, et al. Autophagy promotes tumor cell survival and restricts necrosis, inflammation, and tumorigenesis. *Cancer Cell* 2006; 10:51-64; PMID:16843265; <http://dx.doi.org/10.1016/j.ccr.2006.06.001>
30. Maiuri MC, Tasdemir E, Ciriello A, Morselli E, Vencio JM, Carnuccio R, Kroemer G. Control of autophagy by oncogenes and tumor suppressor genes. *Cell Death Differ.* 2009; 16:87-93; PMID:18806760; <http://dx.doi.org/10.1038/cdd.2008.131>
31. Karantza-Wadsworth V, Patel S, Kravchuk O, Chen G, Mathew R, Jin S, White E. Autophagy mitigates metabolic stress and genome damage in mammary tumorigenesis. *Genes Dev.* 2007; 21:1621-35; PMID:17606641; <http://dx.doi.org/10.1101/gad.1565707>
32. Dang CV, Kim JW, Gao P, Yustein J. The interplay between MYC and HIF in cancer. *Nat. Rev. Cancer.* 2008; 8:51-6; PMID:18046334; <http://dx.doi.org/10.1038/nrc2274>
33. Ma Y, Hendershot LM. The role of the unfolded protein response in tumour development: friend or foe? *Nat. Rev. Cancer* 2004; 4:966-77; PMID:15573118; <http://dx.doi.org/10.1038/nrc1505>
34. Meister S, Schubert U, Neubert K, Herrmann K, Burger R, Gramatzki M, Hahn S, Schreiber S, Wilhelm S, Herrmann M, et al. Extensive immunoglobulin production sensitizes myeloma cells for proteasome inhibition. *Cancer Res.* 2007; 67:1783-92; PMID:17308121; <http://dx.doi.org/10.1158/0008-5472.CAN-06-2258>
35. Cascio P, Oliva L, Cerruti F, Mariani E, Pasqualetto E, Cenci S, Sitia R. Dampening Ab responses using proteasome inhibitors following in vivo B cell activation. *Eur. J. Immunol.* 2008; 38:658-67; PMID:18253932; <http://dx.doi.org/10.1002/eji.200737743>
36. Neubert K, Meister S, Moser K, Weisel F, Maseda D, Amann K, Wiethe C, Winkler TH, Kalden JR, Manz RA, et al. The proteasome inhibitor bortezomib depletes plasma cells and protects mice with lupus-like disease from nephritis. *Nat. Med.* 2008; 14:748-55; PMID:18542049; <http://dx.doi.org/10.1038/nm1763>
37. Hideshima T, Bradner JE, Wong J, Chauhan D, Richardson P, Schreiber SL, Anderson KC. Small-molecule inhibition of proteasome and aggresome function induces synergistic antitumor activity in multiple myeloma. *Proc. Natl. Acad. Sci. U S A.* 2005; 102:8567-72; PMID:15937109; <http://dx.doi.org/10.1073/pnas.0503221102>
38. Kawaguchi T, Miyazawa K, Moriya S, Ohtomo T, Che XF, Naito M, Itoh M, Tomoda A. Combined treatment with bortezomib plus bafilomycin A1 enhances the cytotoxic effect and induces endoplasmic reticulum stress in U266 myeloma cells: crosstalk among proteasome, autophagy-lysosome and ER stress. *Int. J. Oncol.* 2011; 38:643-54; PMID:21174067
39. Santo L, Hideshima T, Kung AL, Tseng JC, Tamang D, Yang M, Jarpe M, van Duzer JH, Mazitschek R, Ogier WC, et al. Preclinical activity, pharmacodynamic, and pharmacokinetic properties of a selective HDAC6 inhibitor, ACY-1215, in combination with bortezomib in multiple myeloma. *Blood* 2012; 119:2579-89; PMID:22262760; <http://dx.doi.org/10.1182/blood-2011-10-387365>
40. Vogl DT, Stadtmayer EA, Tan KS, Heitjan DF, Davis LE, Pontiggia L, Rangwala R, Piao S, Chang YC, Scott EC, et al. Combined autophagy and proteasome inhibition: a phase 1 trial of hydroxychloroquine and bortezomib in patients with relapsed/refractory myeloma. *Autophagy* 2014; 10: 1380-90; PMID:24991834; <http://dx.doi.org/10.4161/auto.29264>
41. Boya P, Reggiori F, Codogno P. Emerging regulation and functions of autophagy. *Nat. Cell Biol.* 2013; 15:713-20; PMID:23817233; <http://dx.doi.org/10.1038/ncb2788>
42. Moscat J, Diaz-Meco MT. p62 at the crossroads of autophagy, apoptosis, and cancer. *Cell* 2009; 137:1001-4; PMID:19524504; <http://dx.doi.org/10.1016/j.cell.2009.05.023>
43. Komatsu M, Ichimura Y. Physiological significance of selective degradation of p62 by autophagy. *FEBS Lett.* 2010; 584:1374-8; PMID:20153326; <http://dx.doi.org/10.1016/j.febslet.2010.02.017>
44. Korolchuk VI, Menzies FM, Rubinsztein DC. Mechanisms of cross-talk between the ubiquitin-proteasome and autophagy-lysosome systems. *FEBS Lett.* 2010; 584:1393-8; PMID:20040365; <http://dx.doi.org/10.1016/j.febslet.2009.12.047>
45. Rodriguez A, Durán A, Selloum M, Champy MF, Diez-Guerra FJ, Flores JM, Serrano M, Auwerx J, Diaz-Meco MT, Moscat J. Mature-onset obesity and insulin resistance in mice deficient in the signaling adapter p62. *Cell Metab.* 2006; 3:211-22; PMID:16517408; <http://dx.doi.org/10.1016/j.cmet.2006.01.011>
46. Ralston SH, Langston AL, Reid IR. Pathogenesis and management of Paget's disease of bone. *Lancet* 2008; 372:155-63; PMID:18620951; [http://dx.doi.org/10.1016/S0140-6736\(08\)61035-1](http://dx.doi.org/10.1016/S0140-6736(08)61035-1)
47. Korolchuk VI, Mansilla A, Menzies FM, Rubinsztein DC. Autophagy inhibition compromises degradation of ubiquitin-proteasome pathway substrates. *Mol Cell* 2009; 33:517-27; PMID:19250912; <http://dx.doi.org/10.1016/j.molcel.2009.01.021>
48. Komatsu M, Waguri S, Koike M, Sou, YS, Ueno T, Hara T, Mizushima N, Iwata J, Ezaki J, Murata S, et al. Homeostatic levels of p62 control cytoplasmic inclusion body formation in autophagy-deficient mice. *Cell* 2007; 131:1149-63; PMID:18083104; <http://dx.doi.org/10.1016/j.cell.2007.10.035>
49. Riley BE, Kaiser SE, Shaler TA, Ng, AC, Hara T, Hipp MS, Lage K, Xavier RJ, Ryu KY, Taguchi K, et al. Ubiquitin accumulation in autophagy-deficient mice is dependent on the Nrf2-mediated stress response pathway: a potential role for protein aggregation in autophagic substrate selection. *J. Cell Biol.* 2010; 191:537-52; PMID:21041446; <http://dx.doi.org/10.1083/jcb.201005012>
50. Chen S, Zhou L, Zhang Y, Leng Y, Pei XY, Lin H, Jones R, Orłowski RZ, Dai Y, Grant S. Targeting SQSTM1/p62 Induces Cargo-Loading Failure and Converts Autophagy to Apoptosis via NBK/Bik. *Mol Cell Biol.* 2014; 34:3435-49; PMID:25002530; <http://dx.doi.org/10.1128/MCB.01383-13>
51. Huang da W, Sherman BT, Lempicki RA. Systematic and integrative analysis of large gene lists using DAVID bioinformatics resources. *Nat. Protoc.* 2009; 4:44-57; PMID:19131956; <http://dx.doi.org/10.1038/nprot.2008.211>